© 2024. Published by The Company of Biologists Ltd | Journal of Cell Science (2024) 137, jcs261164. doi:10.1242/jcs.261164

RESEARCH ARTICLE

SPECIAL ISSUE: CELL AND TISSUE POLARITY

Steroid hormone signaling synchronizes cell migration machinery, adhesion and polarity to direct collective movement

Mallika Bhattacharya and Michelle Starz-Gaiano*

ABSTRACT

Migratory cells – either individually or in cohesive groups – are critical for spatiotemporally regulated processes such as embryonic development and wound healing. Their dysregulation is the underlying cause of formidable health problems such as congenital abnormalities and metastatic cancers. Border cell behavior during *Drosophila* oogenesis provides an effective model to study temporally regulated, collective cell migration *in vivo*. Developmental timing in flies is primarily controlled by the steroid hormone ecdysone, which acts through a well-conserved, nuclear hormone receptor complex. Ecdysone signaling determines the timing of border cell migration, but the molecular mechanisms governing this remain obscure. We found that border cell clusters expressing a dominant-negative form of ecdysone receptor extended ineffective protrusions. Additionally, these clusters had aberrant spatial distributions of E-cadherin (E-cad), apical domain markers and activated myosin that did not overlap. Remediating their expression or activity individually in clusters mutant for ecdysone signaling did not restore proper migration. We propose that ecdysone signaling synchronizes the functional distribution of E-cadherin, atypical protein kinase C (aPKC), Discs large (Dlg1) and activated myosin post-transcriptionally to coordinate adhesion, polarity and contractility and temporally control collective cell migration.

KEY WORDS: *Drosophila*, Border cells, Cell polarity, Collective cell migration, Steroid hormone

INTRODUCTION

Stereotypic cell migration occurs in normal animal development, whereas dysregulated migratory cells contribute to diseases such as metastatic cancer, embryonic malformations and inflammatory diseases (Blackley et al., 2021; Friedl and Mayor, 2017; Roberto and Emery, 2022; Shellard and Mayor, 2019; Yamamoto et al., 2023). Migration in eukaryotes can be classified into individual cell migration or collective cell migration. Although mechanically distinct, these modes of movement involve intricate spatiotemporal coordination of molecules that are often conserved between species and migratory mechanisms. Typically, the detection of external stimuli triggers internal, cell-autonomous responses leading to directional migration. The migratory response can be broadly divided into two steps – orientation, which primes the cell towards a particular direction, and translocation, the physical movement of the cell. Orientation of polarized cells in response to external cues requires the modulation of existing cell polarities to allow cells to migrate. Translocation necessitates the extension of dynamic, actin-rich protrusions and changes in cell–substrate adhesion that allow the cell to pull itself forward. An added requisite of collective cell migration is coordination within the group, often through stable cell–cell adhesion, to establish supracellular polarities such as leading or lagging edge determination and organized protrusive behaviors (Etienne-Manneville, 2012; Friedl and Mayor, 2017; Shellard and Mayor, 2019; Theveneau and Mayor, 2013; Theveneau et al., 2010, 2013; Veeman et al., 2016). How these regulatory processes are synchronized to occur correctly in space and time is an important issue for understanding developmental biology and disease broadly.

Border cell migration during *Drosophila melanogaster* oogenesis (Fig. 1A–C) provides an excellent platform to study collective cell migration, due in part to transparent ovarian tissues, a characterized genome and the availability of robust tools for genetic manipulation (Aman and Piotrowski, 2010; Giedt and Tootle, 2023; Hudson and Cooley, 2014; Montell et al., 2012). Moreover, *Drosophila* has highly conserved gene networks with fewer family members than in vertebrates, which narrows the focus to key, conserved genetic regulators. The border cell cluster arises as six to eight cells within the anterior follicular epithelium of an egg chamber (Fig. 1A) (Montell et al., 2012). The cluster consists of two non-motile polar cells surrounded by motile border cells, the latter being specified at stage 8 of oogenesis (Montell et al., 2012; King, 1970). After a coordinated shape change to form a compact and cohesive group, the border cell cluster detaches from the epithelium and migrates between germline cells, called nurse cells, towards the oocyte at stage 9 (Fig. 1B,C). This posterior migration is completed in approximately 4 h by stage 10 (Bianco et al., 2007; Prasad and Montell, 2007; Tekotte et al., 2007), and timely migration to the oocyte is required to form a fertilizable egg (King, 1970). Genetic and imaging studies have uncovered both molecular and biophysical aspects of border cell migration *in vivo*. The migratory cluster retains some characteristics of epithelial cells, such as apical and basal polarity, while adopting migratory properties, including dynamic shape changes and leading or lagging edge polarity, consistent with properties of collective cell migration (reviewed in Montell et al., 2012; Peercy and Starz-Gaiano, 2020; Veeman et al., 2016).

Border cell translocation occurs via the extension of actin-based protrusions that adhere to their substrate, i.e. nurse cells. Protrusions that adhere successfully ‘grapple and pull’ the cluster forward (Bianco et al., 2007). These protrusions are then retracted as the lagging edge of the cluster contracts (Aranjuez et al., 2016; Bianco et al., 2007; Lamb et al., 2020; Plutoni et al., 2019; Poukkula et al., 2011). Cycles of protrusion extension, adhesion and retraction repeat to continue forward movement. Chemoattractant signaling biases protrusions in the appropriate direction towards the oocyte (Bianco et al., 2007; Prasad and Montell, 2007). This and the

Department of Biological Sciences, University of Maryland Baltimore County, 1000 Hilltop Circle, Baltimore, MD 21250, USA.

*Author for correspondence (starz@umbc.edu)

M.S.-G., 0000-0002-0855-0715

Handling Editor: David Bryant
Received 11 March 2023; Accepted 23 January 2024

Journal of Cell Science (2024) 137, jcs261164. doi:10.1242/jcs.261164

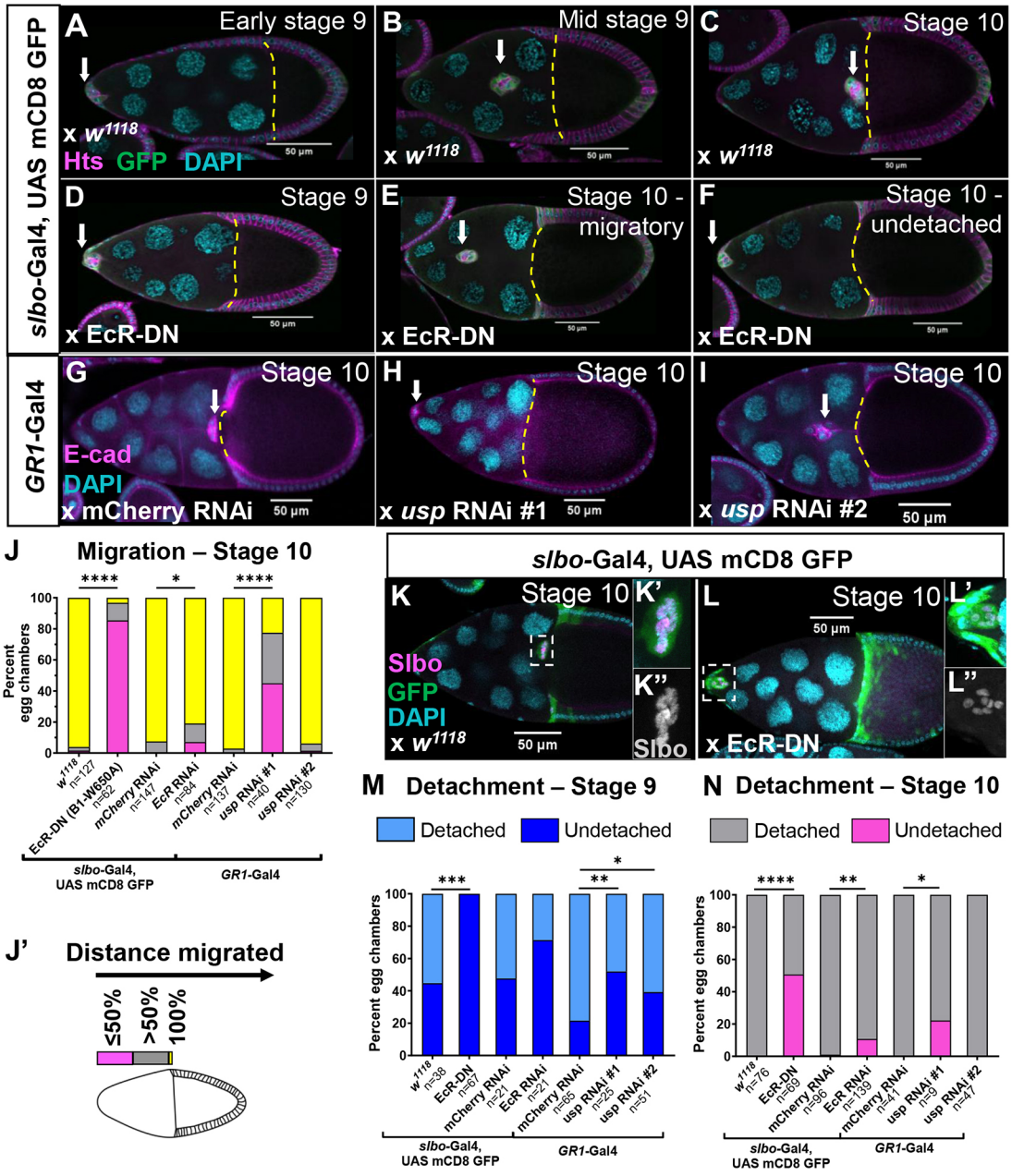

Fig. 1. Reduced ecdysone signaling disrupts border cell migration. (A–C) Normal migration in control egg chambers over stages 9 (A,B) and 10 (C). The anterior is to the left in all egg chambers. (D–F) Expression of the EcR-DN construct (UAS-EcR-B1-W650A) in border cells delays migration. (D) A late stage 9 egg chamber with an undetached border cell cluster. (E,F) At stage 10, EcR-DN-expressing border cells sometimes migrate but are delayed (E, compare to C) or not detached (F). In A–F, border cells express membrane-tethered GFP (green) due to *slbo*-Gal4; Hu-li tai shao (Hts, magenta) immunolabeling marks cell membranes; and DAPI (cyan) marks nuclei. (G) A control stage 10 egg chamber with wild-type border cell migration. In G–I, E-cadherin (E-cad, magenta) immunolabeling is enriched in the border cell membranes; DAPI (cyan) marks nuclei. (H,I) Downregulation of *usp* in follicle cells [*GR1*-Gal4 and TRiP. JF02546 (#1) and TRiP. HMS01620 (#2)] leads to detachment defects (H) or delayed migration (I). In A–I, white arrows indicate the border cell clusters and yellow dashed lines show the oocyte boundary. (J,J′) Quantification of the penetrance of migration defects (J), based on the distance migrated by stage 10, as depicted in J′. (K–L″) Slbo (magenta; grayscale in insets in K″,L″) immunolabeling shows expression in both control (K) and EcR-DN-expressing (L) border cells along with GFP (green). (M,N) Quantification of the detachment of border cells from the epithelium at stages 9 (M) and 10 (N). For J,M,N, *n*=number of egg chambers; **P*<0.05, ***P*<0.01, ****P*<0.001 and *****P*<0.0001 measured by Fisher's exact test. All scale bars: 50 µm.

presence of nurse cells around the cluster limits the directions in which protrusions are extended (Dai et al., 2020; Fulga and Rørth, 2002; Prasad and Montell, 2007; Stonko et al., 2015). Thus, stabilized, forward-facing protrusions are important functionally for promoting forward movement and steering border cell migration, whereas uncoordinated or ectopic protrusions can severely hinder migration.

Molecularly, protrusive forces in border cells are generated through actin polymerization and re-organization of filaments mediated by Rac regulation (Campanale et al., 2022; Gates et al., 2009; Kim et al., 2011; Murphy and Montell, 1996; Plutoni et al., 2019; Wang et al., 2010; Zhang et al., 2011), whereas contraction forces, needed for protrusion and lagging edge retractions and cluster shape maintenance, require activation of myosin regulatory

Journal of Cell Science (2024) 137, jcs261164. doi:10.1242/jcs.261164

light chain (MRLC) (Aranjuez et al., 2016; Edwards and Kiehart, 1996; Majumder et al., 2012; Mishra et al., 2019; Zeledon et al., 2019). In border cell clusters, the homophilic adhesion protein E-cadherin [E-cad; encoded by *shotgun* (*shg*)] maintains the organization of the cluster while promoting adhesion to nurse cells (Cai et al., 2014; Chen et al., 2020; Mishra et al., 2019; Niewiadomska et al., 1999). Migratory border cells redistribute E-cad and Armadillo (Arm, fly homolog of β-catenin) from their epithelial distribution in adherens junctions to end up with widespread high levels between cells of the cluster and lower levels at the periphery in contact with nurse cells (Bai et al., 2000; Niewiadomska et al., 1999; Peifer and Wleschaus, 1990). E-cad is required in border cells, polar cells and nurse cells for collective migration (Cai et al., 2014; Chen et al., 2020; Niewiadomska et al., 1999). Cai et al. (2014) suggest that border cell adhesion with germline cells feeds back on actin re-organization, promoting protrusion extension. Importantly, cortical myosin distribution is dependent on E-cad, and clusters expressing a phosphomimetic form of MRLC are less protrusive and more rounded (Mishra et al., 2019; Chen et al., 2021). Moreover, E-cad overexpression blocks migration, suggesting that strict maintenance of E-cad levels occurs during border cell migration (Schober et al., 2005).

While migrating collectively, border cells also coordinate their behaviors by maintaining apicobasal polarity and cell–cell adhesion within the cluster. Initial compaction, detachment and migration of border cell clusters results in relocalization but not complete loss of epithelial polarity proteins (Bastock and Strutt, 2007; Felix et al., 2015; Pinheiro and Montell, 2004; Woods et al., 1996). Reducing the function of core apicobasal polarity components, such as Discs large (Dlg1), Scribble (Scrib) and atypical protein kinase C (aPKC), or other Par complex proteins, results in border cell migration defects, as does ectopic localization of polarized proteins (Anllo and Schüpbach, 2016; Bastock and Strutt, 2007; Campanale et al., 2022; Felix et al., 2015; Goode and Perrimon, 1997; Pinheiro and Montell, 2004; Stephens et al., 2018; Wang et al., 2018; Woods et al., 1996). These results indicate that the migratory cluster requires the proper localization of apicobasal polarity complexes, although their spatial organization is dynamic throughout migration. Thus, tight regulation is required between cell polarity, adhesion and actomyosin network remodeling for optimal migration, but how events are coordinated temporally is unclear.

The initial movement of border cells is triggered by steroid hormone signaling (Bai et al., 2000; Cherbas et al., 2003; Hackney et al., 2007), but the mechanism for this is unknown. Flies have a single steroid hormone called ecdysone, which temporally regulates many developmental processes, including most changes during metamorphosis (Riddiford, 1993). Ecdysone binds to a heterodimeric receptor containing Ecdysone receptor (EcR) and Ultraspiracle (Usp), which translocates to the nucleus and acts in conjunction with co-activators or co-repressors to regulate transcription. Both EcR and Usp have conserved mammalian homologs (Dawson and Xia, 2012; Hu et al., 2003; Thomas et al., 1993; Yao et al., 1993; Zhao et al., 2014). Ecdysone is required for oogenesis and is produced autonomously in each egg chamber (Domanitskaya et al., 2014). Hormone titers rise in late stage 8 egg chambers as border cells are specified (Buszczak et al., 1999; Riddiford, 1993), and loss of EcR signaling in border cells blocks migration (Bai et al., 2000; Cherbas et al., 2003; Hackney et al., 2007). Increasing ecdysone signaling through the administration of active hormone or the expression of a constitutively active coactivator of EcR, Taiman (Tai), along with premature border cell specification, results in precocious migration (Bai et al., 2000; Jang et al., 2009). Thus, ecdysone signaling appears to be necessary and sufficient for the temporal regulation of border cell migration. Although some transcriptional targets of EcR signaling have been identified in migratory cells (Jang et al., 2009; Manning et al., 2017), the critical targets that trigger collective border cell migration are not known.

Here, we explicate the role of steroid hormone signaling in border cell migration. When ecdysone signaling was blocked in border cells, most clusters did not move, but we found that they still maintained border cell identity. These cells extended protrusions with reduced functionality. Additionally, in the absence of ecdysone signaling, border cells had aberrant localization of E-cad, aPKC and Dlg1, indicating defective cell adhesion and apicobasal polarity, and irregular phospho-myosin distribution, leading to abnormal cluster shape and contractility. The changed localization domains of E-cad, Dlg1, aPKC and phospho-myosin distribution did not overlap or complement each other, suggesting that they are not interdependent. Additionally, genetically changing the levels of these proteins did not mimic the distribution patterns that arose due to disruptions of ecdysone signaling, and compensatory changes in E-cad and phospho-myosin levels were not sufficient to remediate the incomplete migration of mutant clusters or induce proper protein localization patterns. These data suggest that hormone signaling is critical for the precise, dynamic spatiotemporal regulation of key adhesion and polarity proteins and it acts through multiple target mechanisms. Thus, we propose a model wherein ecdysone signaling acts at a specific time to promote collective movement by coordinating the two steps of migration – orientation and translocation – by synchronizing cell polarity and adhesion, which localizes remodeling of the actomyosin network to enable directional, effective protrusions and coordinated, timely collective cell movement.

RESULTS

Ecdysone signaling promotes border cell detachment and migration

To elucidate the role of ecdysone signaling in border cell migration, we used three different genetic tools to reduce signaling. First, we expressed a dominant-negative form of the receptor that prevents transcriptional activation (EcR-B1-W650A, also referred to EcR-DN; Cherbas et al., 2003) specifically in the border cells. At stage 9, control clusters rounded up, detached from the anterior of the egg chamber and migrated towards the oocyte (Fig. 1A–C). When using a border cell-specific Gal4, *slbo*-Gal4, to express EcR-DN, most clusters did not migrate at stage 9 (Fig. 1D). As previously observed with this and other dominant-negative transgenes (Cherbas et al., 2003; Hackney et al., 2007; Jang et al., 2009; Manning et al., 2017), stage 10 EcR-DN-expressing clusters either failed to migrate or migrated partially, but almost never exhibited complete migration, in contrast to the behavior of controls (compare Fig. 1C with Fig. 1E,F). Over 90% of EcR-DN-expressing clusters migrated less than 50% of the normal distance (Fig. 1J). We found similar results by reducing ecdysone signaling through expression of an RNAi construct (*EcR* RNAi, Ni et al., 2011) (Fig. 1J; Fig. S1A–C). Consistent with previous reports, this also resulted in migration defects, albeit weaker ones (Fig. 1J; Fig. S1A–C) (Wang et al., 2020). We confirmed that the EcR protein level was reduced in *EcR* RNAi-expressing border cells (Fig. S1B–D). We suspect that expression of the dominant-negative receptor results in a stronger phenotype than that of RNAi because it occludes transcription-mediated signaling by EcR more completely. Second, we expressed and validated two separate RNAi constructs that target *usp* (Ni et al., 2011) (Fig. S1E), which encodes the heterodimerization partner of

Journal of Cell Science (2024) 137, jcs261164. doi:10.1242/jcs.261164

EcR. Expressing a *usp* RNAi construct using a pan-follicle cell-specific Gal4 active from stage 4 of oogenesis, *GR1*-Gal4 (Gupta and Schüpbach, 2003; Tran and Berg, 2003), resulted in some migration defects compared to controls (Fig. 1G–J; Fig. S1A). Over 50% of stage 9 *usp* RNAi-expressing clusters were delayed, whereas over 70% of clusters did not complete migration in stage 10. Notably, this cross yielded low numbers of viable offspring, suggesting that the reduction of *usp* is partially lethal and that viable adults were 'escapees' that partially suppressed the RNAi effect. Last, we expressed EcR-DN in border cells at an earlier stage using c306-Gal4, in combination with a temperature-sensitive repressor of Gal4 activity, ts-Gal80, to overcome lethality (Fig. S1H–K; Materials and Methods). Post border cell specification, when c306-Gal4 is active, we saw strong migration defects (Fig. S1H,I). Given the failure of border cell migration when ecdysone signaling was blocked, we wondered whether border cell identity was disrupted. Notably, we found normal expression of the key regulator and indicator of border cell fate, the Slow border cells (Slbo) protein (Montell et al., 1992), in border cells expressing EcR-DN (Fig. 1K, L; Fig. S1F,G). This indicates that the border cells remain specified correctly and the migration defects observed were specific to ecdysone signaling and separate from defects in cell identity.

We next assessed whether ecdysone signaling regulates the timing of migration solely by regulating the time of detachment of the cluster from the anterior epithelium. We quantified the frequency of undetached clusters at stages 9 and 10 when ecdysone signaling was reduced. Detachment occurred during early stage 9 and, at this stage, about half of the control border cell clusters were detached (Fig. 1M). In contrast, 100% of EcR-DN-expressing clusters were undetached at stage 9 with *slbo*-Gal4 (Fig. 1M), and 90% with c306-Gal4 (Fig. S1J). We observed milder but notable defects in clusters expressing *EcR* or *usp* RNAi (Fig. 1M). By stage 10, at least 98% of control clusters were detached (Fig. 1N). However, 50.7% of EcR-DN-expressing clusters remained undetached at stage 10 when controlled with *slbo*-Gal4 (Fig. 1N), and 84% with c306-Gal4 (Fig. S1K). Clusters expressing *EcR* or *usp* RNAi also had increases in detachment defects (Fig. 1N). Importantly, EcR-DN-expressing clusters that did detach still did not complete migration (Fig. 1J).

Ecdysone signaling enables functional protrusions

As about half of all EcR-DN-expressing clusters detached and migrated some distance by stage 10, they were clearly motile. But these clusters did not complete migration, so they likely had additional defects in migratory behaviors. To characterize the EcR-DN clusters more closely, we used live imaging using membrane-tethered GFP to visualize the cluster and membrane protrusions (mCD8–GFP and/or PLCδ-PH–EGFP) (Fig. 2A–C) (Sawant et al., 2018; Verstreken et al., 2009). Detached EcR-DN-expressing clusters migrated significantly more slowly than control clusters (Fig. 2D, Movies 1–4). As cluster shape and perimeter reflect migratory behavior, we analyzed border cell cluster shape by fitting it to an ellipse and calculating the aspect ratio of the major and minor axes (see Materials and Methods). Control migratory clusters at stage 9 tended to be rounded up instead of elongated (Aranjuez et al., 2016), giving them a mean aspect ratio near 1.34, whereas stage 10 clusters that had completed migration adopted a more flattened/elongated shape, with a ratio of 1.85 (Fig. 2E; Fig. S2A–B‴). As EcR-DN-expressing clusters did not detach at stage 9, making it hard to assess morphology, we restricted our analysis to detached EcR-DN-expressing clusters at stage 10. These had a significantly lower mean aspect ratio than typical for this stage (1.44; Fig. 2E; Fig. S2C–C‴) and resembled the rounded shapes of control clusters in a similar migratory position at stage 9. Migratory EcR-DN-expressing clusters also had highly irregular peripheral membranes at stage 10 with many small protrusions along their perimeter (Fig. 2F; Fig. S2C‴,C‴). These protrusions resembled those observed at stage 9 in controls, although they were smaller and less organized. In contrast, control stage 10 clusters tended to have a smoother peripheral surface (Fig. 2F; Fig. S2B‴,B‴). To quantify this difference and to control for the size of the cluster, we measured the perimeter of the cluster normalized to its area. EcR-DN-expressing stage 10 clusters had a higher mean perimeter-to-area ratio than that of control clusters at the same stage (0.32 compared to 0.25) (Fig. 2F) and were more similar to stage 9 controls (0.29). This supports the idea that EcR-DN-expressing migratory stage 10 clusters have delayed migratory behaviors, consistent with the idea that ecdysone temporally regulates both detachment and migration.

The defects in motility and shape of EcR-DN-expressing clusters could be explained by inefficient cytoskeletal protrusion dynamics, so we examined the protrusions more closely. Control clusters extended protrusions primarily in the direction of migration (Fig. 2A–A‴), and forward protrusions were typically longer in length and lived longer (Fig. 2H,I) (Bianco et al., 2007; Fulga and Rørth, 2002; Poukkula et al., 2011; Prasad and Montell, 2007). Clusters expressing PLCδ-PH–EGFP along with EcR-DN had enhanced detachment defects, so were usually undetached at late stage 9 but did extend protrusions (Fig. 2B–B‴). Stage 10 control clusters were at the oocyte border, whereas EcR-DN, PLCδ-PH–EGFP-expressing clusters extended few or no protrusions (Fig. 2C–C‴) and barely translocated. We quantified differences in the average number of protrusions extended (Fig. 2G), the maximal length of protrusions (Fig. 2H) and the lifetime of each protrusion (Fig. 2I) at stage 9. The direction of protrusion extension was classified by dividing the cluster into four quadrants, based on the position in the image: forward, lateral – top, lateral – bottom, and rear (Fig. 2J). The average number of protrusions extended by controls and EcR-DN, PLCδ-PH–EGFP-expressing clusters were comparable (Fig. 2G), indicating that ecdysone signaling is not required generally to form protrusions. However, the forward-facing protrusions – those likely to be the most functional and productive for migration – extended by EcR-DN-expressing clusters were on average shorter than those extended by control clusters (Fig. 2H) and were retracted faster, as evidenced by shorter lifetimes (Fig. 2I). In contrast, protrusions extended laterally by EcR-DN-expressing clusters were more stable: they were longer on average, with longer lifetimes than those of lateral protrusions in controls (Fig. 2H,I). As EcR-DN, PLCδ-PH–EGFP-expressing clusters rarely moved from the anterior, we could not quantify rear-facing protrusions. These data suggest that although EcR-DN-expressing clusters actively extended protrusions at stage 9, they were less functionally efficient and contributed less to forward translocation. This indicates that the migration defects of clusters with reduced ecdysone signaling are due to delayed or unsuccessful detachment from the epithelium and to defects in protrusions.

Ecdysone signaling regulates polarized distribution of the adhesion complex component E-cad

Migration and structural integrity of the border cell cluster require maintenance of optimal levels of E-cad (Cai et al., 2014; Niewiadomska et al., 1999; Schober et al., 2005). E-cad must be frequently remodeled at the cluster periphery to allow protrusion extension, adhesion and retraction. Given the aberrant protrusion

Journal of Cell Science (2024) 137, jcs261164. doi:10.1242/jcs.261164

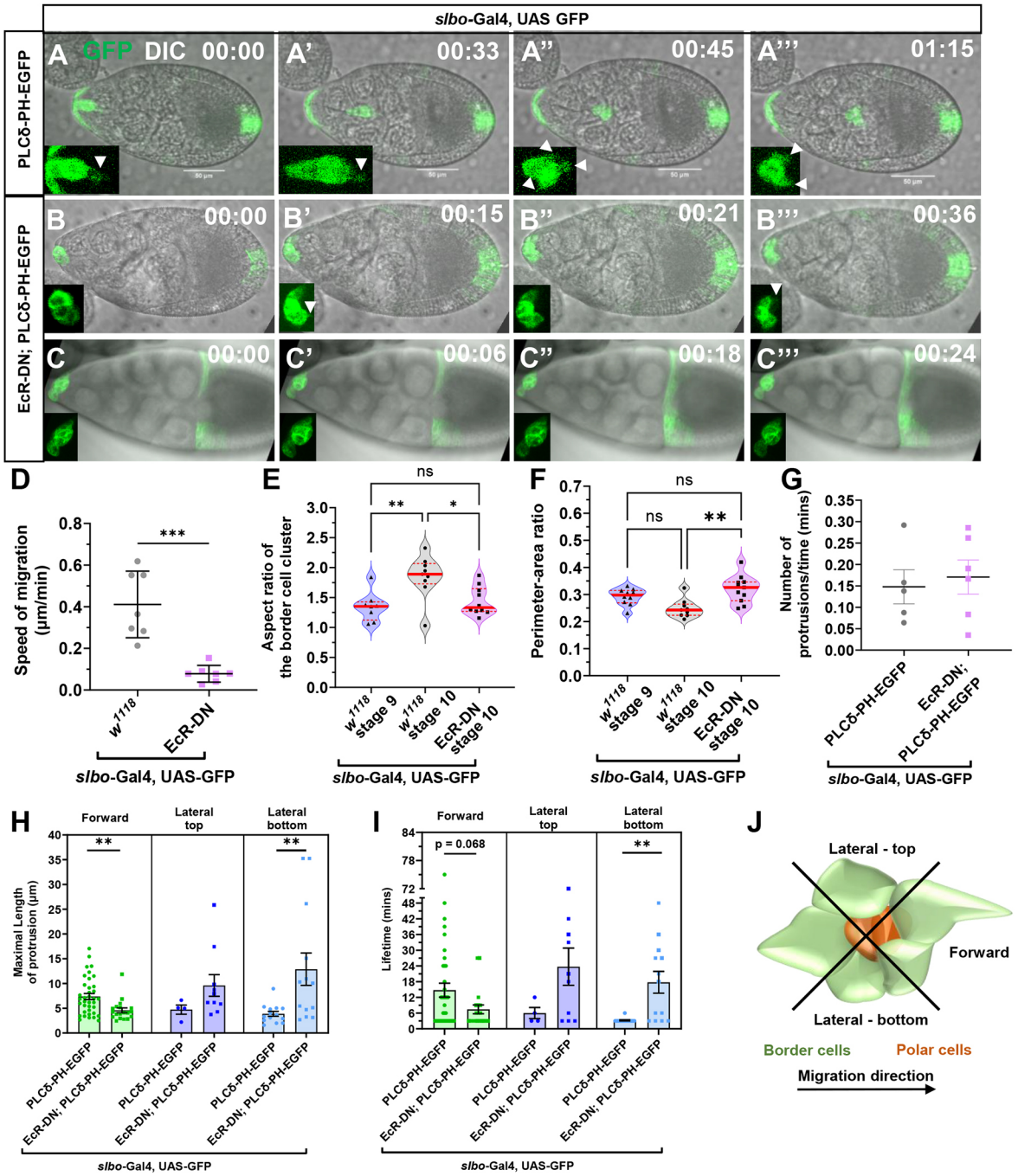

Fig. 2. EcR-DN-expressing border cells have protrusion defects. (A–C‴) Screenshots from sum-intensity projection timelapse videos of a control egg chamber exhibiting wild-type border cell migration (A–A‴) and of egg chambers expressing EcR-DN in the border cells with incomplete migration at stages 9 (B–B‴) and 10 (C–C‴). GFP (green) marks the border cells and differential interference contrast (DIC) shows egg chambers; time is in minutes. Insets show border cell protrusions (arrowheads). Scale bars: 50 µm. (D) Quantification of migration speeds of control and detached EcR-DN-expressing clusters. Each data point represents an individual cluster. ***P<0.001 from a two-tailed unpaired t-test. (E) Aspect ratio analysis of clusters of the genotypes and stages indicated. (F) Perimeter normalized to area analysis of clusters from the genotypes and developmental stages indicated. Statistical significance for E,F was measured by one-way ANOVA with Tukey's multiple comparison test: ns, not significant; *P<0.05; **P<0.01. Red lines on violin plots represent mean±s.e.m.; outlines display the spread of data. Each data point is an individual cluster. (G) Quantification of protrusions extended during timelapse imaging in stage 9 egg chambers. (H,I) Quantification of maximal lengths (H) and lifetimes (I) of protrusions extended classified by direction. Each data point represents a protrusion. n≥5 stage 9 egg chambers. **P<0.01 or precise P-value is given from a two-tailed unpaired t-test. Graphs show the mean±s.e.m. (J) Quadrants of a border cell cluster used for protrusion analysis in H,I.

dynamics in EcR-DN-expressing clusters, we reasoned that changes in E-cad localization or levels might contribute to these defects.

We examined E-cad localization in control, EcR-DN-expressing and E-cad (*shg*) RNAi-expressing clusters (Fig. 3A–D). In migratory control clusters (stage 9), E-cad intensity was the highest at the apical face of the cluster in polar cells and at border cell–polar cell interfaces and was enriched along basolateral locations between border cells (Fig. 3A–A‴). Most border cell

Journal of Cell Science (2024) 137, jcs261164. doi:10.1242/jcs.261164

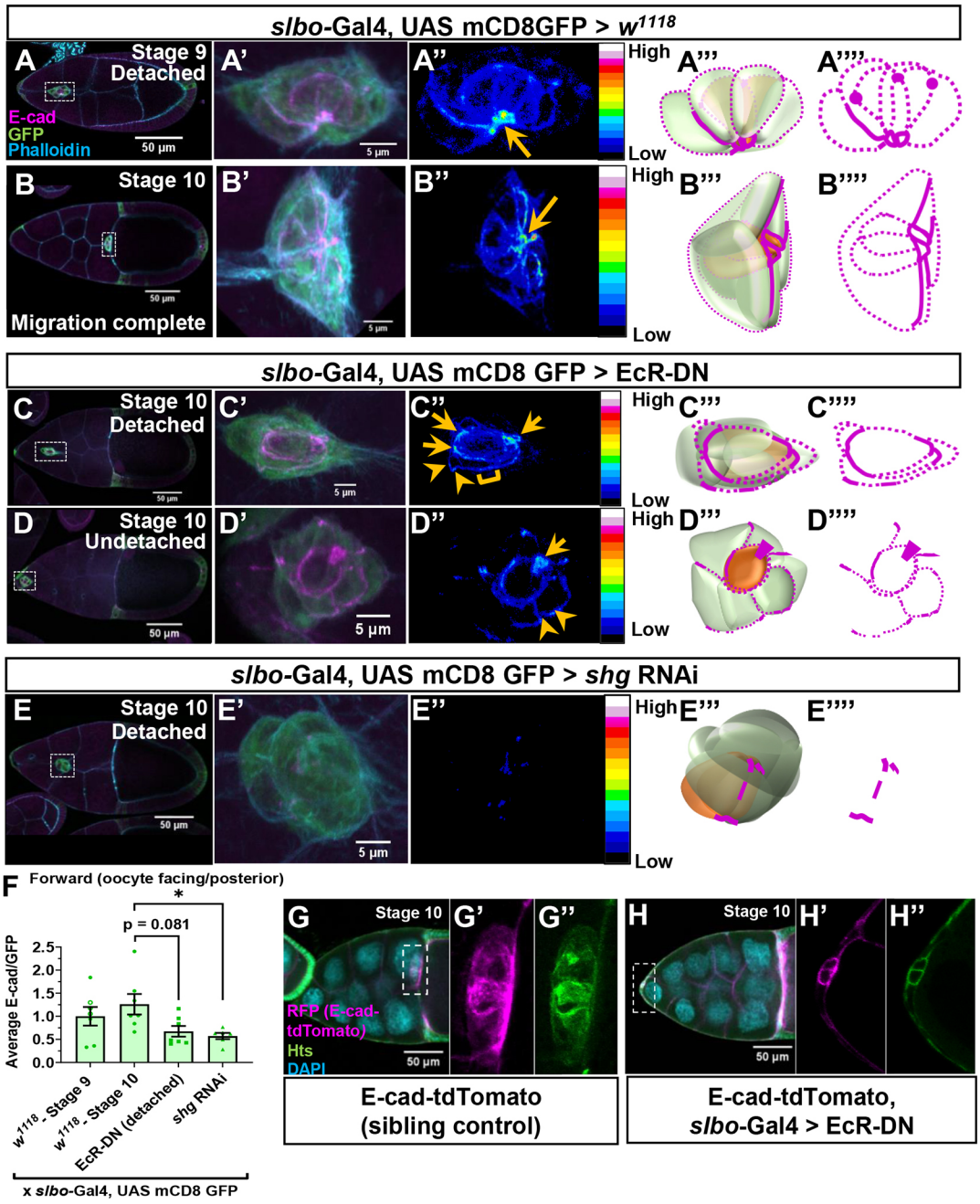

Fig. 3. EcR-DN-expressing clusters have irregular E-cad distribution. (A,B) Control egg chambers stained with antibodies recognizing E-cad (magenta) and GFP (green), with fluorescent phalloidin labeling F-actin (cyan). (A′,B′) Enlarged image of border cell cluster. (A″,B″) Maximum-intensity projections of border cells. E-cad expression is pseudocolored with an intensity-based LUT. Orange arrows mark the highest concentrations of E-cad in the apical domain of polar cells. (A‴–B⁗) Schematic of the border cell cluster and its E-cad distribution in magenta. Bold lines represent high E-cad intensity. (C–D″) Egg chambers showing E-cad distribution in EcR-DN-expressing clusters (boxed), enlarged in C′,D′, for detached (C) or undetached (D) cases, shown as a maximum-intensity projections in C″,D″. The intensity-based LUT shows E-cad levels. Orange arrows mark domains of high E-cad at polar cells. Arrowheads and the bracket mark irregular, high E-cad distribution along cluster peripheral membranes. (C‴–D⁗) Schematic of border cells and E-cad distribution (magenta). (E–E⁗) E-cad distribution in a detached cluster expressing *shg* (*E-cad*) RNAi in the egg chamber (E), with the maximum-intensity projection (E′), intensity levels (E″) and schematics (E‴,E⁗). (F) Quantification of average E-cad levels normalized to GFP, by antibody staining, on the forward-facing face. Measurements from each egg chamber are plotted; bars show the mean±s.e.m. *P<0.05 or exact P-value is shown from one-way ANOVA with Tukey's multiple comparison test. (G–H″) Egg chambers expressing E-cad–tdTomato stained with antibodies recognizing RFP (magenta, for E-cad–tdTomato, G′,H′), Hts (green, G″,H″), and labeled with DAPI (cyan) for control (G) and EcR-DN-expressing (H) border cells. Images are representative of more than eight similar egg chambers imaged in detail from each of three experiments.

membranes at the outer periphery of the cluster had lower signal intensity. In control stage 10 clusters that had completed migration, there was increased signal intensity at membranes where border cells met the oocyte, and at the apical region of border cell–polar cell membranes (Fig. 3B–B⁗). Because *slbo*-Gal4 is expressed in outer border cells only, expression of EcR-DN with this line did not autonomously affect apical E-cad enrichment in the central polar cells. However, E-cad was irregularly distributed at border

Journal of Cell Science (2024) 137, jcs261164. doi:10.1242/jcs.261164

cell–nurse cell edges of both detached and undetached EcR-DN-expressing clusters (Fig. 3C–D‴). Some peripheral edges had scattered areas of E-cad enrichment, whereas a subset had noticeably lower E-cad localization (forward cell in Fig. 3C″ and rear cell in Fig. 3D″). Additionally, instead of a single region of high intensity at the apical face, we sometimes detected two regions along the border cell–polar cell membranes enriched for E-cad (Fig. 3C″) and lower localization at a subset of the peripheral edges, even when the border cell cluster had not completely detached (Fig. 3D–D″). These data suggest that ecdysone signaling regulates the distribution of E-cad at border cell membranes. Alternatively, loss of ecdysone signaling might reduce the expression of E-cad, indirectly leading to its irregular distributions. However, when we knocked down E-cad (*shg* RNAi) in border cell clusters, we saw a distinct effect from EcR-DN: very low levels of E-cad expression generally with very restricted signal at border cell–polar cell membranes (Fig. 3E–E‴).

We next assayed E-cad distribution further. Using an anti-E-cad antibody (Oda et al., 1994), we quantified staining intensity at the peripheral border cell faces of stage 10 clusters: forward-facing, rear-facing and lateral (Fig. 3F; Fig. S3A–D). We measured the average intensity at each face and normalized it to that of membrane-tethered GFP at the same location. In this quantification, E-cad RNAi (*shg* RNAi) resulted in lower E-cad intensities than those of wild-type controls. Although EcR-DN-expressing clusters also sometimes had visibly lower staining, we did not measure statistically significant differences in average intensity at any face or in overall corrected total cell fluorescence when comparing detached, partially migrated, stage 10 EcR-DN-expressing clusters to control clusters at the same stage or at a similar migratory position (stage 9) (Fig. S3E). We also examined protein distribution using a transgenic line expressing E-cad fused to the fluorescent protein tdTomato (Huang et al., 2009). Although the E-cad antibody detects the extracellular domain only, E-cad–tdTomato can reveal cytoplasmic E-cad. We did not see a notable change in the distribution of cytoplasmic E-cad in EcR-DN-expressing clusters (Fig. 3G,G′ versus Fig. 3H,H′), although these clusters did not coalesce or migrate well and membrane-localized E-cad levels appeared low in this genotype. As these clusters rarely detached and control clusters abutted the high E-cad expression at the oocyte, it precluded measurement of equivalent peripheral faces of the cluster between the mutant and controls. Overall, we conclude that although EcR-DN-expressing clusters did not have dramatic differences in E-cad levels, they had abnormal E-cad distribution at peripheral membranes.

Homophilic cadherin adhesions bridge the actin cytoskeleton across neighboring cells, coupling them mechanically (Cai et al., 2014; Mège and Ishiyama, 2017; Wang et al., 2020). As we observed changes in E-cad distribution as well as protrusion and migration defects in EcR-DN-expressing clusters, we next examined actin levels. We stained egg chambers and separately quantified intensity levels of an actin-binding protein, Hu-li tai shao (Hts), and those of an F-actin marker, fluorescently labeled phalloidin (Fig. S3F–I). Hts highly localized to the border cell cluster and other follicle cells but not to nurse cell membranes. Average Hts and phalloidin staining intensity levels, normalized to those of GFP, were comparable in control and EcR-DN-expressing clusters across migratory stages (Fig. S3H,I), suggesting that loss of ecdysone signaling does not dramatically change the levels of F-actin.

Given the changed E-cad distribution, we wondered whether the distribution and/or expression of other cadherins was also perturbed in response to blocking ecdysone signaling. Cells can upregulate N-cadherin (N-cad or CadN) expression in response to E-cad downregulation (Oda et al., 1998; Schäfer et al., 2014). In egg chambers, N-cad expression is widespread in follicle cell membranes but decreases from stage 7 onwards and is undetectable at stage 10 (Grammont, 2007). We did not find changes in the pattern of N-cad distribution in EcR-DN-expressing clusters (Fig. S3J–M). Taken together, these data suggest that ecdysone signaling specifically promotes the even peripheral distribution of E-cad in the border cell cluster.

Ecdysone signaling restricts localization of the apical proteins aPKC and Dlg1

Epithelial cells establish apicobasal polarity through the asymmetric distribution of polarity complexes and junctional proteins, which in turn modulate cytoskeletal elements. The irregular phenotypes of EcR-DN-expressing clusters suggested that these mutant border cells have defects in polarity. To test this, we examined two markers of apical polarity, aPKC and Dlg1. aPKC is an integral member of protein complexes that define the apical domain of cells (Buckley and St Johnston, 2022). Although remodeled at the start of migration, the proper positioning of aPKC is important for directional protrusion dynamics and efficient border cell migration (Pinheiro and Montell, 2004; Wang et al., 2018). Immunofluorescence analysis on maximum-intensity projections of control stage 10 clusters showed higher aPKC levels at apical border cell–polar cell membranes in contact with the oocyte (Fig. 4A–A‴), whereas border cell–border cell membranes had lower signal (Fig. 4A–A″). EcR-DN-expressing clusters had an expanded domain of aPKC distribution at most cell membranes compared to controls (Fig. 4C–C‴). To quantify differences in aPKC localization, we drew a line around the circumference of the border cell cluster, starting and ending at the high apical region of polar cell expression, and measured staining intensities in control and EcR-DN-expressing clusters (Fig. 4B,D; Fig. S4). Although this varied by cluster, in aggregate, the normalized distributions showed a dramatic expansion of aPKC localization such that it was abnormally higher in lateral and basal domains in EcR-DN-expressing stage 10 clusters (Fig. 4D) compared to that in control clusters of the same stage (Fig. 4B) or in similar migratory positions (stage 9, Fig. S4K).

Dlg1 is also involved in the establishment and maintenance of apicobasal polarity in the follicular epithelia and is present at contacts between border cells (Goode and Perrimon, 1997; Woods and Bryant, 1991; Woods et al., 1996). Hackney et al. (2007) observed increased Dlg1 accumulation in follicle cell clones expressing EcR-DN in older-stage egg chambers and in egg chambers mutant for ecdysone production. Thus, we expected a similar upregulation in the mutant border cells. Immunofluorescence analysis of control stage 10 clusters showed higher Dlg1 at apical border cell–polar cell membranes in contact with the oocyte (Fig. 4E–E‴), whereas border cell–border cell membranes had very low signal (Fig. 4E–E‴). EcR-DN-expressing clusters had an expanded domain of Dlg1 signal at border cell–border cell membranes compared to stage 9 and 10 controls (Fig. S4A; Fig. 4G–G‴). The intensely stained Dlg1 region at the border cell–polar cell membranes appeared to be largely unaffected in EcR-DN-expressing clusters (Fig. 4G″). Quantification of the normalized signal intensity at the circumference of the border cell clusters showed a slight expansion of the apical localization of Dlg1 in EcR-DN-expressing clusters and a larger range of expression intensities (Fig. 4H) compared to that in control clusters at the same

Journal of Cell Science (2024) 137, jcs261164. doi:10.1242/jcs.261164

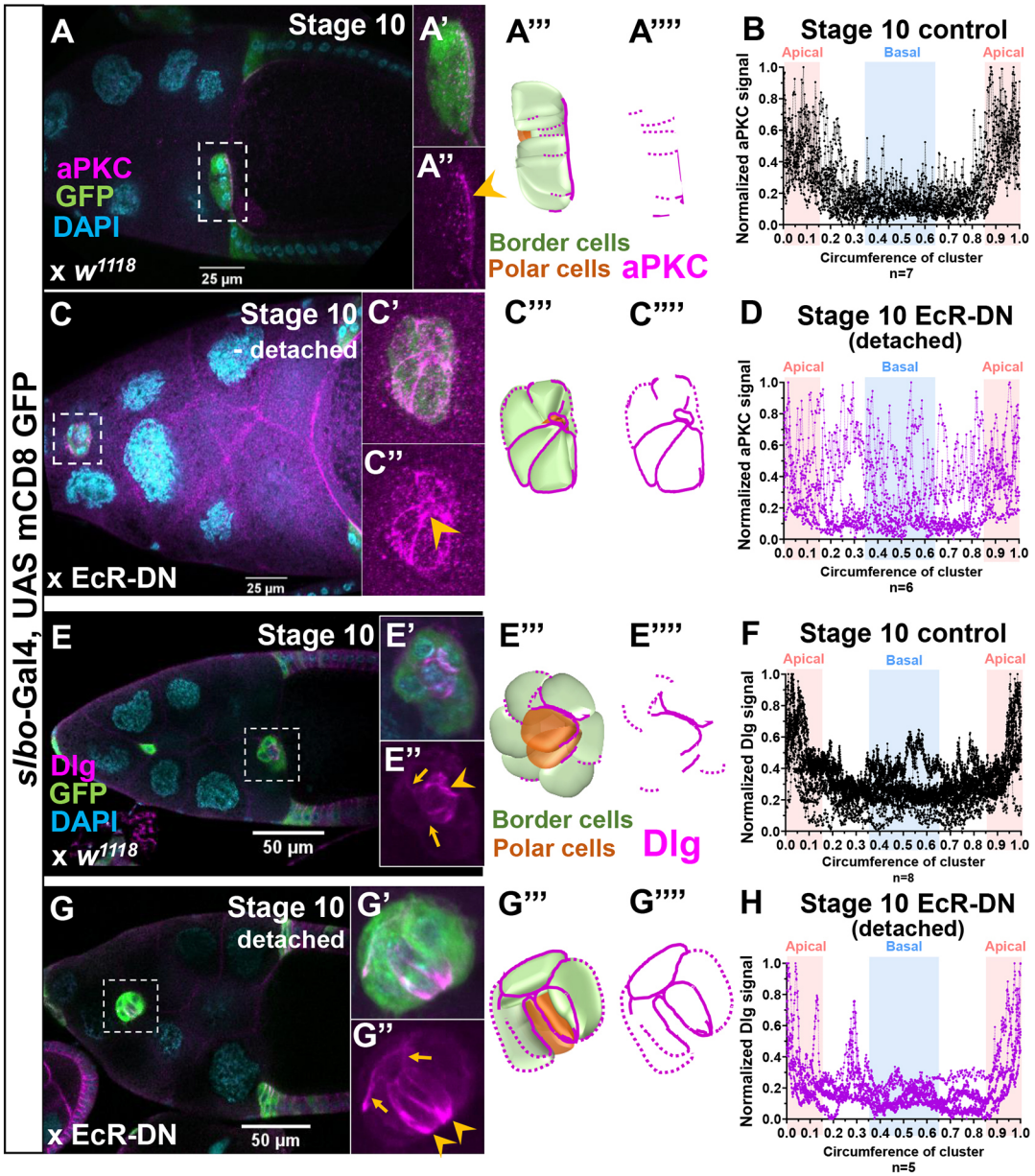

Fig. 4. EcR-DN-expressing clusters mislocalize apical polarity proteins. (A–A″,C–C″) Normal control (A) or EcR-DN-expressing (C) egg chambers stained for aPKC (magenta) and GFP (green) expression, and with DAPI (cyan). White dashed boxes show the area enlarged as maximum-intensity projections in insets. (A″,C″) Arrowheads indicate high aPKC intensity in apical domains near polar cells, which expands baso-laterally in mutant clusters (C″). (A‴,A⁗,C‴,C⁗) Schematics of border cell clusters with high levels of aPKC in magenta. (B,D) Intensity measurements of peripheral aPKC expression measured around the cluster circumference. Graphs show levels for six to seven egg chambers for control or EcR-DN-expressing clusters at stage 10 (see also Materials and Methods and Fig. S4). Apical regions are shaded in pink and basal regions are shaded in blue. (E–E″,G–G″) Control (E) or EcR-DN-expressing (G) egg chambers stained with antibodies against Dlg1 (magenta) and GFP (green), and with DAPI (cyan). Boxed regions are magnified in insets. (E″) The arrowhead indicates high Dlg1 intensity in polar cell apical domains; arrows point to membranes with faint Dlg1 signal. (G) EcR-DN-expressing border cells show basally expanded Dlg1 expression (arrows in G″; arrowheads indicate apical polar cell domain). (E‴–G⁗) Schematics of border cell clusters with high levels of Dlg1 in magenta. (F,H) Intensity measurements of peripheral Dlg1 expression plotted for five to eight egg chambers for control or EcR-DN-expressing clusters at stage 10.

stage (Fig. 4F) or at similar migratory positions (stage 9, Fig. S4L). We saw similar, aberrant localization of Dlg1 and aPKC, respectively, using *EcR* RNAi (Fig. S4A–C″) or expression of another dominant-negative construct (EcR-B1-F645A, Fig. S4D–E″). The expanded Dlg1 distribution did not appear to be due to a general increase in expression, as it differed from the pattern observed in *dlg1* overexpression experiments, which showed higher cytoplasmic and membrane intensities of Dlg1 (Fig. 4G versus Fig. S4G,H). However, we observed ectopic protrusions in stage 10 clusters overexpressing *dlg1* (Fig. S4G′,G″), and similar ectopic protrusions have been observed when aPKC is overactivated (Wang et al., 2018), suggesting that an expanded Dlg1 domain could contribute to the ectopic protrusions in EcR-DN-expressing clusters (Fig. S2C). Overall, the data indicate that ecdysone signaling is needed to maintain proper aPKC and Dlg1 localization in the border cell cluster.

Journal of Cell Science (2024) 137, jcs261164. doi:10.1242/jcs.261164

The mislocalization of apical proteins in EcR-DN-expressing clusters suggested that the distribution of other polarity proteins could also be affected. Dlg1 colocalizes with septate junction proteins although it is not required for the establishment or maintenance of septate junctions (Oshima and Fehon, 2011; Rice et al., 2021; Woods and Bryant, 1991). Core septate junction proteins, remodeled in migrating border cells, are required for movement (Alhadyian et al., 2021). We assayed a core component, Coracle (Cora), as ecdysone signaling regulates its localization in the wing disc epithelium (DaCrema et al., 2021). In both control and EcR-DN-expressing clusters, Cora showed the same pattern of distribution (Fig. S4I–J″) (Felix et al., 2015). This suggests that ecdysone signaling does not generally regulate the localization of all proteins associated with polarity, nor does it merely delay their localization, but instead is specifically needed for proper Dlg1 and aPKC distribution.

Ecdysone signaling promotes proper spatiotemporal phospho-myosin distribution

Border cell clusters dynamically regulate activated, phosphorylated non-muscle myosin II (p-MyoII) to maintain cell shape, resist compression, detach from the anterior epithelium and retract protrusions during migration (Aranjuez et al., 2016; Edwards and Kiehart, 1996; Majumder et al., 2012; Mishra et al., 2019; Plutoni et al., 2019; Zeledon et al., 2019; Chen et al., 2021). Additionally, non-phosphorylated, cortical myosin distribution is dependent in part on E-cad (Mishra et al., 2019). The aberrant E-cad, aPKC and Dlg1 distribution domains coupled with the extension of fewer long and stable forward-directed protrusions by EcR-DN-expressing clusters suggested that the adhesion-mediated feedback loop between nurse cells and border cells could be impeded. If true, this would affect actomyosin organization at border cell membranes.

Thus, we examined p-MyoII distribution in EcR-DN-expressing clusters using an antibody directed against human phospho-Myosin Regulatory Light Chain (pMRLC), which recognizes the fly homolog encoded by *spaghetti squash* (*sqh*) (Karess et al., 1991; Lamb et al., 2021; Majumder et al., 2012). At stage 9, control clusters showed intense pMRLC puncta localized to the base of protrusions, at border cell–border cell contacts, and at the rear of the migrating cluster (Fig. 5A–A″) (Majumder et al., 2012; Mishra et al., 2019). pMRLC co-localized with strong phalloidin staining, consistent with the idea that the actomyosin network contributes actively to migration or cluster integrity at these regions (Fig. 5A–A″). At stage 10, faint pMRLC signals were visible throughout the cluster (Fig. 5D–D″). In the example in Fig. 5D, a stronger pMRLC-stained region is visible at the rear. EcR-DN-expressing clusters had some pMRLC puncta at stage 9 (Fig. 5B–B″) but, strikingly at stage 10, strong pMRLC signals were visible along peripheral border cell membranes (Fig. 5E–E″) and sometimes appeared as discrete puncta. Phalloidin staining of EcR-DN-expressing clusters matched the pattern of pMRLC distribution.

We quantified pMRLC foci and their distribution at stages 9 and 10, eliminating foci below a minimum size threshold (0.1 μm^2) (Fig. 5C,F; Fig. S5A–D). We did not observe any significant differences in the total number or average size of individual pMRLC foci between controls and EcR-DN-expressing clusters across stages (Fig. S5C,D). However, we observed distinct temporal patterns of pMRLC localization in EcR-DN-expressing clusters compared to that in controls. Stage 9 control clusters that had migrated less than halfway to the oocyte had polarized pMRLC distribution, with more foci in the forward quadrant, compared to that in stage 10 clusters (Fig. 5C). In contrast, EcR-DN-expressing clusters had a significantly lower proportion of forward foci at stage 9 than at stage 10. These mutant clusters also had a lower proportion of forward foci compared to those in control clusters in a similar migratory position (stage 9, ≤50% migrated, Fig. 5C). In the lateral top quadrant, control stage 9 clusters (≤50% or >50% migrated) had comparable or fewer foci compared to stage 10 clusters, but this trend was reversed in EcR-DN-expressing clusters, which had a significantly higher proportion of lateral foci at stage 9 relative to that at stage 10 (Fig. 5F). A similar but milder trend was observed in the lateral bottom quadrant (Fig. S5A). In the rear quadrant, control stage 9 and 10 clusters had comparable proportions, but EcR-DN stage 9 clusters tended to have slightly fewer foci than older clusters (Fig. S5B). Thus, relative to controls, the temporal patterns of EcR-DN-expressing clusters in the four compartments were reversed. This suggests that the main difference in the mutant clusters is uncoordinated distribution of phospho-myosin within the migratory axis over the migratory timeframe.

Irregular distribution of pMRLC might occur due to mislocalization of the myosin protein or its activation. To study the distribution of myosin, we used a *sqh*-GFP insertion line (Royou et al., 2004). As previously shown, Sqh–GFP was visible in control clusters at cell cortices (Fig. 5G–H‴). Additionally, we observed Sqh–GFP-enriched foci that reflect the location of activated myosin (Fig. 5G″,H″) (Majumder et al., 2012; Royou et al., 2004). Sqh–GFP distribution matched the pattern of enriched phalloidin staining (Fig. 5G″,G‴,H″,H‴). Cortical Sqh–GFP was also visible in stage 9 and 10 EcR-DN-expressing clusters (Fig. 5I–J‴). This suggests that Sqh itself is not mislocalized, but that some other aspect of myosin activation must be altered. Live imaging of EcR-DN-expressing clusters expressing *sqh*-GFP showed periodic Sqh–GFP flashes similar to those in control clusters (Movies 5–7). Thus, it is possible that the rate of phosphorylation and dephosphorylation of myosin is similar in EcR-DN-expressing clusters and controls, but the location of coalescing activated myosin, and thus force transduction, is altered. Taken together, our data indicate that border cell clusters require ecdysone signaling for optimal phospho-myosin distribution and actomyosin network dynamics.

Altering E-cad and activated myosin levels does not remediate migration defects due to reduced ecdysone signaling

EcR-DN-expressing clusters have abnormal distributions of E-cad, aPKC, Dlg1 and phospho-myosin. We wondered whether there were consistent, potentially overlapping, patterns in these altered distributions. To compare patterns, we stained egg chambers expressing *sqh*-GFP with antibodies directed against GFP and E-cad (Fig. 5G–J). In both control and EcR-DN-expressing clusters, Sqh–GFP foci or enriched regions did not consistently overlap with enriched E-cad regions (Fig. 5G,H versus Fig. 5I,J). Next, we immunostained for Dlg1 and phospho-myosin (Fig. S5E–F″) or Dlg1 and E-cad (Fig. S5G–H″) distributions. Again, we did not observe consistent patterns linking ectopic distributions of Dlg1 with phospho-myosin or E-cad. We attempted to rescue the expanded Dlg1 localization domain in EcR-DN-expressing clusters to see whether this suppressed the mutant phenotype, but were unsuccessful in generating the right genotype. As the mislocalized patterns of E-cad, Dlg1 and pMRLC do not change cooperatively, we postulate that ecdysone signaling regulates the distribution of each of these independently.

Finally, we tested whether changing the distribution of E-cad or activated myosin in EcR-DN-expressing clusters alleviated the migration defects. We overexpressed E-cad (*shg*) fused to GFP and found that it enriched at border cell membranes along with some

Journal of Cell Science (2024) 137, jcs261164. doi:10.1242/jcs.261164

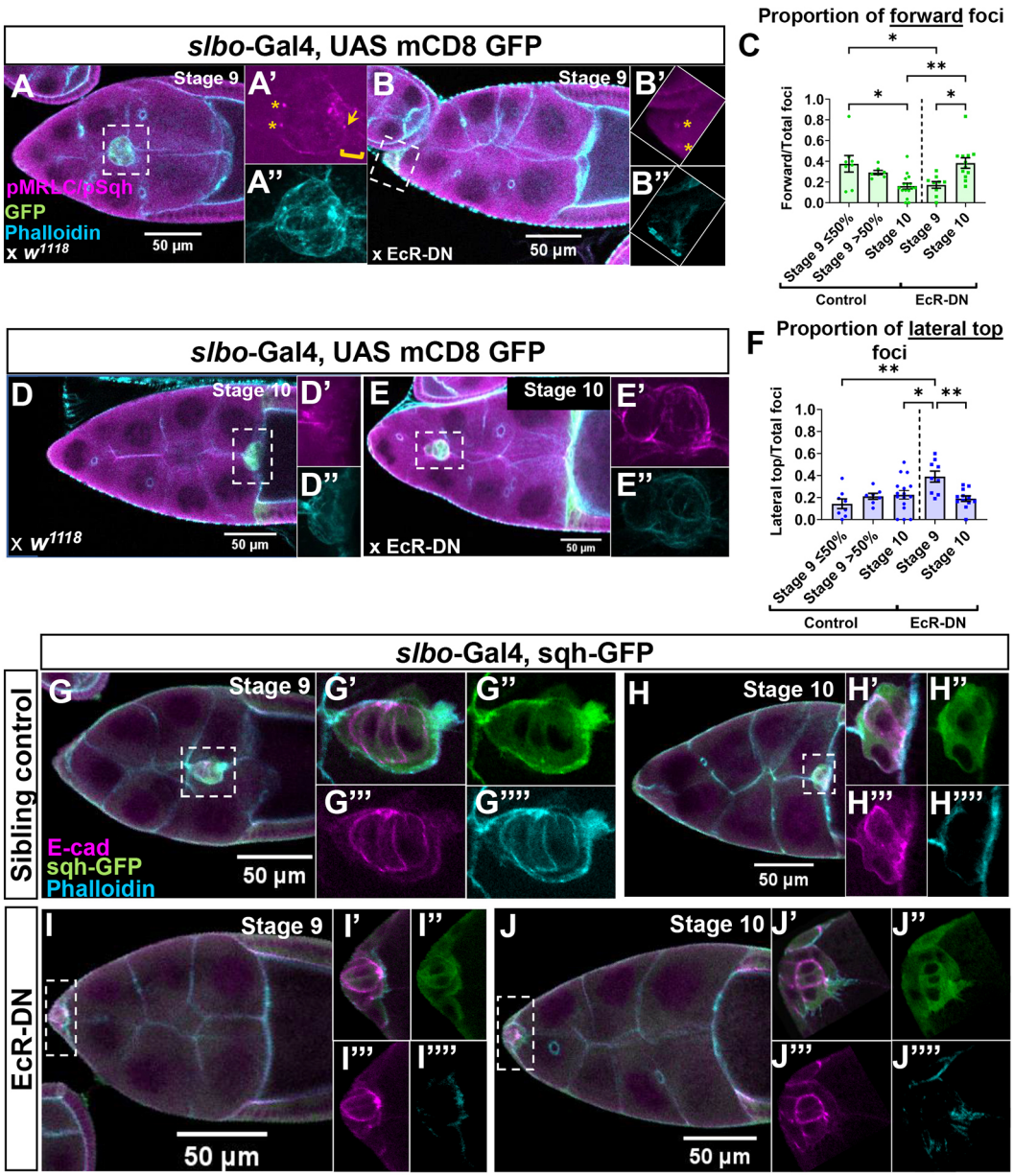

Fig. 5. EcR-DN-expressing clusters have aberrant activated myosin localization. (A–B″,D–E″) Egg chambers stained with antibodies recognizing phospho-myosin regulatory light chain (pMRLC, magenta) and GFP (green), and fluorescent phalloidin (F-actin, cyan). Dashed boxes are enlarged in maximum-intensity projection insets. (A′) In a stage 9 control egg chamber, the arrow points to a pMRLC focus at the base of a protrusion (bracket). Asterisks label pMRLC foci at the rear of the cluster. (B′) EcR-DN-expressing stage 9 border cell cluster. Asterisks mark faint lateral pMRLC foci. (D′) In the stage 10 control, one intensely stained pMRLC region is visible at the rear (anterior) side of the cluster. (E′) In EcR-DN-expressing border cells, pMRLC staining is observed along many membranes. (C,F) Quantification of pMRLC foci in forward (C) and lateral top (F) border cell cluster quadrants (mean ±s.e.m.; **P*<0.05 and ***P*<0.01 from one-way ANOVA with Tukey's multiple comparison test). (G–J″″) Egg chambers stained for antibodies recognizing E-cad (magenta) and GFP (Sqh–GFP, myosin, green), and with fluorescent phalloidin (F-actin, cyan). (G,H) Control Sqh–GFP egg chambers at stages 9 (G) and 10 (H). (I,J) Sqh–GFP egg chambers expressing EcR-DN in the border cells. Images are representative of more than ten egg chambers per genotype imaged in detail.

signal at the cell cortex facing nurse cells (Fig. S6A–A″). Border cell migration is disrupted when E-cad is overexpressed (Schober et al., 2005). Interestingly, co-expression of EcR-DN and *shg*-GFP led to suppression of E-cad levels (Fig. S6C–C″ versus Fig. S6A) but poor border cell migration – resembling EcR-DN expression alone – compared to those in sibling controls (Fig. S6B–B″). Next, to counteract irregular phospho-myosin distribution, we lowered overall myosin levels in EcR-DN-expressing clusters using an RNAi targeting *sqh* (Fig. S6D–E″) or co-expression of an activated form of the regulatory phosphatase, Myosin-binding subunit (Mbs N300, Lee and Treisman, 2004) (Fig. S6F–G″). Lowering myosin levels or altering its activation also did not rescue the migration defect caused by lack of ecdysone signaling (Fig. S6E,G). These results reinforce the idea that ecdysone signaling separately regulates the distribution of E-cad and activated myosin and that it acts through multiple effectors to promote migration.

DISCUSSION

Here, we elucidate regulatory mechanisms of cell migration controlled by steroid hormone signaling. In border cell migration,

Journal of Cell Science (2024) 137, jcs261164. doi:10.1242/jcs.261164

ecdysone signaling was known to be necessary and sufficient for the initial movement of specified cells (Bai et al., 2000; Cherbas et al., 2003; Domanitskaya et al., 2014; Hackney et al., 2007; Jang et al., 2009) but its precise roles in border cell migration were unclear. Putting together our data, we propose a model wherein ecdysone signaling permits migration by restricting the distributions of E-cad, aPKC, Dlg1 and phospho-myosin soon after border cell specification (Fig. 6). This signaling appears to be independent of other signaling pathways, as border cell identity is not affected, and EcR-DN-expressing clusters have distinct morphologies compared to those of other mutants (e.g. overactivation of myosin, Fig. S6H). The successful coordination of cell adhesion, polarity and cluster contractility by EcR in wild-type migratory clusters results in the extension of functional protrusions, facilitating directional migration at the proper developmental time.

Optimal protrusion dynamics are important for directionality and force generation in cell migration (Blackley et al., 2021; Roberto and Emery, 2022). We found that border cell clusters lacking ecdysone signaling extended shorter and shorter-lived forward protrusions while extending longer, more stable protrusions laterally. This suggests that mutant clusters are not just temporally delayed, as they can regulate F-actin to make extensions at the right stage, but they are not able to differentiate the leading and lagging edges to stabilize forward, functional protrusions preferentially. Although our live imaging might miss some short-lived protrusions, such as those observed in fixed clusters (Fig. S2C‴), these protrusions are unlikely to aid in 'grapple and pull' mechanics and thus are probably less productive.

Protrusion stability depends on regulation of cell adhesion and retraction mechanisms, which determine how strongly a protrusion adheres to a substrate and for how long. This prompted us to examine E-cad. Previously, Hackney et al. (2007) noted an increased E-cad intensity in EcR-DN-expressing clusters. In contrast, we observed irregular distributions of E-cad and variable decreases in intensity levels at the cluster periphery. The irregular patterns, orientations and abnormal shapes of mutant clusters made this expression change challenging to quantify. Romani et al. (2009) also observed reduced E-cad levels upon EcR-B1 knockdown in the follicular epithelium. It has been suggested that the organization of E-cad in aggregates, rather than its overall expression levels, impacts local adhesive and tensile forces (Cavey et al., 2008; Hong et al., 2013; Truong Quang et al., 2013). The irregular E-cad distributions that we observed in EcR-DN-expressing border cells might reflect a change in E-cad aggregation dynamics, although our images are not at a resolution that can resolve this. We conclude that ecdysone signaling is required for the appropriate localization of E-cad and that this contributes to

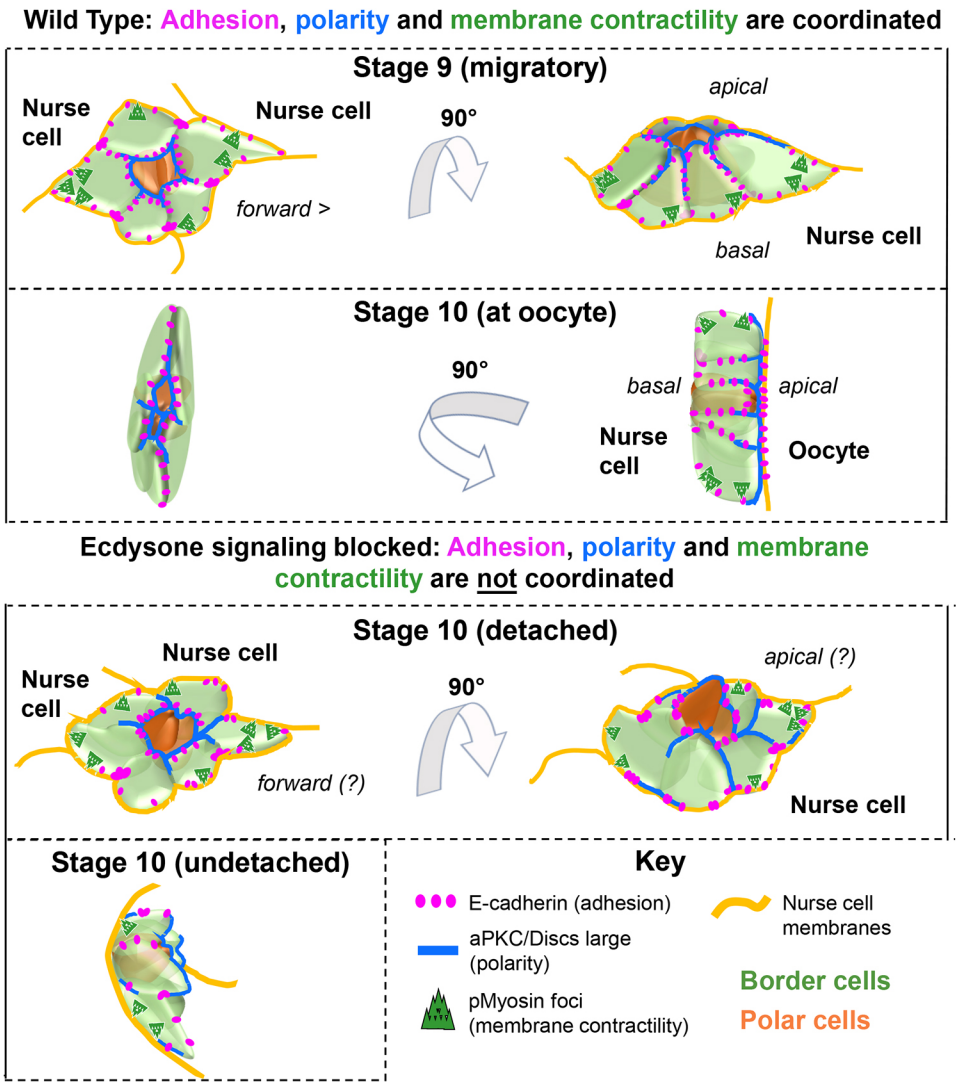

Fig. 6. Ecdysone signaling coordinates adhesion, polarity and local membrane contractility to enable detachment and migration. Schematic depicting E-cad, the apical domain containing aPKC and Dlg1, and pMyosin distribution in border cell clusters in different stages, positions and orientations to show polarity and developmental changes. When ecdysone receptor signaling is blocked, border cell clusters that detach and are migratory at stage 10 have altered localization patterns of the adhesion protein E-cad, poor forward orientation, expanded apical markers and abnormal distribution of activated phospho-myosin compared to those of wild type migratory clusters (stage 9) or wild-type clusters at the same developmental stage. Often, mutant clusters never detach.

Journal of Cell Science (2024) 137, jcs261164. doi:10.1242/jcs.261164

stabilizing productive protrusions. Intriguingly, steroid hormone signaling-mediated maintenance of E-cad expression is commonly observed in mammalian systems. In mouse mammary epithelial cells, estrogen receptor β increases E-cad expression, and loss of this receptor leads to increased internalization and a change in localization of E-cad (Helguero et al., 2008). Similarly, the lactating mammary gland and uterine epithelia show reduced E-cad levels in estrogen receptor β knockout mice (Förster et al., 2002; Wada-Hiraike et al., 2006).

Our results show that ecdysone signaling in border cell migration confines the apical domain of the cells. This aligns with a prior report that EcR-B1 knockdown in the follicular epithelium altered aPKC and Dlg1 distribution domains (Romani et al., 2009). Dlg1 regulates the core septate junction component Cora in some tissues (Bilder et al., 2002; Khadilkar and Tanentzapf, 2019; Tanentzapf and Tepass, 2002), but Dlg1 dynamics are separable from core junction component dynamics (Oshima and Fehon, 2011). Some experiments suggest septate junction proteins are required for border cell migration and are enriched in polar cells (Alhadyian et al., 2021; Felix et al., 2015). However, as we did not see changes in Cora distribution when ecdysone signaling was blocked, we do not believe that the loss of EcR signaling results in a larger area of septate junctions. Instead, we think this reveals a less refined apicobasal polarity in mutant clusters, as seen by aPKC expansion. Our experiments relied on blocking ecdysone signaling in outer border cells because other genetic combinations led to lethality, so residual ecdysone signaling in polar cells likely maintains some polarity and cohesion in the cluster. Nevertheless, our data indicate that disruption of the apicobasal domains in border cells contributes to disrupted migration behaviors. Multiple lines of evidence suggest that migrating collectives maintain and integrate multiple modalities of polarity (e.g. planar polarity or apicobasal polarity), which inform the supracellular front–back polarity changes to the cytoskeletal network and cell–cell adhesions (Ann Mack and Georgiou, 2014; Bazellières et al., 2018; Campanale et al., 2022; Gandalovičová et al., 2016; McDonald et al., 2008; Niewiadomska et al., 1999; Pinheiro and Montell, 2004; Veeman et al., 2016; Wang et al., 2018). Misdistribution of polarity proteins can severely hinder the directionality of protrusion extension and migration. Recently, polarity switching has been shown to be a mechanism of migration and invasion in ovarian cancer and colorectal cancer organoids (Kawata et al., 2022; Okuyama et al., 2016). These cell clusters have an apical-in and basal-out conformation that resembles apicobasal polarity in border cell clusters. Thus, the restriction of polarity proteins to specific domains by steroid hormone signaling might be important in a variety of contexts.

Interestingly, we found that ecdysone signaling also confines the distribution of activated phospho-myosin. In border cell clusters, asymmetrical activated myosin distribution is critical for protrusion retraction in the front of the cluster and the retraction at the cluster rear. Phosphorylation of myosin is tightly regulated in migratory border cells by Rho kinase (Rok) and myosin phosphatase. The broader distribution of pMRLC staining in EcR-DN-expressing clusters resembles that of overexpression of Rok or knockdown of a regulatory subunit of myosin phosphatase, Mbs (Majumder et al., 2012). Thus, the defects in EcR-DN expressing clusters might arise from mislocalization of Rok or myosin phosphatase, although we were unable to rescue the defects by activating the phosphatase. Rok and Mbs function complementarily to coordinate the contractions in the front and rear of the cluster (Aranjuez et al., 2016; Majumder et al., 2012; Mishra et al., 2019; Chen et al., 2021). The changes in the proportion of activated myosin foci in the front and lateral compartments when ecdysone signaling is reduced compared to control clusters could help to explain the migratory defects we observed. Abnormal distribution of activated myosin in EcR-DN-expressing clusters likely contributes to their defective shapes due to changes in local contractility. Prior work shows that genetic manipulations to increase activation of myosin result in increased detachment defects (Majumder et al., 2012), which is similar to what we saw when EcR signaling was disrupted. Thus, the misdistribution of activated myosin in border cells with reduced ecdysone signaling might partially explain the detachment defects. Interestingly, computational modeling of the effect of actomyosin force on E-cad aggregation shows that fewer but larger aggregates are more probable in the presence of high actomyosin forces (Chen et al., 2021). The increased proportion of pMRLC foci laterally at stage 9 and in the forward compartment at stage 10 might mimic the higher actomyosin forces modeled and could potentially contribute to irregular E-cad distribution. We did not see consistent overlap between cortical myosin aggregations and E-cad in EcR-DN-expressing clusters, but the pMRLC antibody staining protocol did not allow for simultaneous detection of E-cad. Overall, it appears that ecdysone signaling synchronizes the contributions of E-cad, apicobasal polarity, forward–rear polarity and the distribution of activated myosin to promote migration, which suggests that changing any individual component in clusters with reduced ecdysone signaling is not likely to rescue the mutant phenotype. The combinatorial coordination by ecdysone signaling is also reflected in the much stronger phenotype when ecdysone receptor signaling is disrupted, compared to the incompletely penetrant phenotypes of failure to detach or incomplete migration when E-cad or myosin activity regulators are knocked down individually (Chen et al., 2020; Majumder et al., 2012).

How ecdysone signaling molecularly coordinates migration machinery is not yet clear. Although disruptions of this signaling cause migration delays, the phenotypic differences between the wild type and mutant suggest that it is not simply acting as a timer. Other than cluster shape and position, stage 10 EcR-DN-expressing clusters have unique protein distribution phenotypes that do not resemble wild-type clusters at the same stage or in a similar migratory position. We speculate that following an initial migration delay, potentially due to an onset of problems with multiple protein distributions in EcR-DN-expressing clusters, the high level of disorganization within the cluster precludes any recovery that could lead to resumption of normal migration. It is possible that apicobasal polarity distortion in EcR-DN-expressing clusters could cause the other defects we saw, such as miscoordinated protrusions and adhesion defects. However, we do not think this is likely as some polarized protein distributions remained unaffected (Hts, N-cad and Cora) in the mutants; thus, poor apicobasal polarity probably only partially contributes to the phenotypes. As ecdysone receptor is a transcription factor, it is conceivable that it could regulate E-cad, aPKC, Dlg1 and myosin expression transcriptionally. However, a microarray analysis did not reveal these or any canonical migration-regulatory proteins as downstream targets in border cells (Manning et al., 2017). Thus, we anticipate that EcR regulates migration indirectly by controlling protein localization domains via currently unknown transcriptional targets. Alternatively, EcR might post-transcriptionally regulate E-cad, apical components and myosin and/or regulators of these proteins, for example, through microRNA expression or changes in post-translational modifications to affect their localization and/or turnover. An interesting recent study shows that ecdysone signaling alters lipid regulation (Li et al., 2023), providing an intriguing possibility that ecdysone signaling mutants

Journal of Cell Science (2024) 137, jcs261164. doi:10.1242/jcs.261164

could alter membrane composition and protein localization at the cell surface. Lastly, as signaling pathways do not function in isolation, the permissive cue from ecdysone signaling must work in cooperation with other motility-instructing signaling pathways (e.g. Janus kinase/Signal transducer and activator of transcription guidance factors and Hippo signaling) to tailor border cell migration (Montell et al., 2012; Saadin and Starz-Gaiano, 2016), so more work is needed to understand these interactions. Overall, we show a previously unreported regulatory mechanism of collective cell migration kinetics by a nuclear hormone receptor. Many nuclear hormone receptors are associated with diseases, so fully understanding their actions might be a useful tool for targeting therapeutics in the future (Kittler et al., 2013; Polvani et al., 2014).

MATERIALS AND METHODS

Fly stocks and husbandry

Flies were raised on standard cornmeal-molasses food and were cultured under standard conditions (25°C) unless otherwise noted. For genetic crosses, virgin females of the appropriate genotype were collected at 18°C for 2–7 days before crossing with males. Most crosses were established and maintained at 25°C except for crosses containing the temperature-sensitive expression construct tsGal80. tsGal80 suppresses Gal4 activity in a temperature-dependent manner. Crosses with this construct were established and maintained at 18°C to repress Gal4 activity because continuous expression of EcR-DN with c306 is lethal. Flies of the appropriate genotypes were then shifted to 29°C overnight to suppress Gal80, permit Gal4 activity and induce expression of the EcR dominant-negative construct. We observed poor survival when *usp* RNAi was expressed with *GR1*-Gal4 compared to outcrossed controls, worse with P{TRiP. JF02546} compared to P{TRiP. HMS01620}. Detailed genotypes are listed in Table S1.

Ovary dissection

Prior to dissection, 2- to 7-day-old flies were transferred to yeast-supplemented food at 25°C or 29°C and maintained at the temperature for different periods of time depending on their genotype, as follows. Unless otherwise noted, experiments that included Gal4 transgenic lines were incubated at 29°C for 15–17 h to maximize stage 8–10 egg chamber yield and Gal4 function. Other genotypes were incubated at 25°C for 18–20 h. Ovaries were extracted from female flies anesthetized under CO_2 into dissection medium [1× Schneider's *Drosophila* medium (Thermo Fisher Scientific, 21720-001), 10% fetal bovine serum (Thermo Fisher Scientific/Gibco, 16000) and 0.6% penicillin/streptomycin (Thermo Fisher Scientific/Gibco, 15140148)] and dissected further into ovarioles. When dissecting multiple genotypes, ovarioles to be used for immunofluorescence were stored on ice prior to fixation. Ovarioles to be used for live imaging were dissected in insulin-supplemented dissection medium (see below) and were stored at room temperature (RT).

Immunostaining and live imaging of egg chambers

Following dissection, ovarioles were washed once with dissection medium before using them for either immunofluorescence or live imaging. For a detailed list of antibodies and dyes used, refer to Table S2. Immunostaining was performed as per the following protocol for all antibodies except the one directed against phospho-myosin (see below). Briefly, dissected samples were fixed in 4% paraformaldehyde (Electron Microscopy Sciences, 15710) diluted in 1× PBS for 10 min at RT. Fixed ovarioles were rinsed once and washed two times with NP40 buffer [0.05 M Tris-HCl, pH 7.4, 0.15 M NaCl, 0.5% Nonidet P-40 (Igepal CA-630, Sigma-Aldrich) and 1 mg/ml bovine serum albumin (BSA)]. Samples were then incubated with the respective primary antibody and/or phalloidin diluted in NP40 buffer for one or two overnight incubations at 4°C. Following primary antibody incubation, samples were washed two to three times and incubated with secondary antibody (1:400) and phalloidin if indicated (1:50) overnight at 4°C or for 2–3 h at RT. Samples were washed once more before incubation with DAPI (1:1000 diluted in NP40 buffer) for 10 min at RT to stain DNA to visualize the nuclei. This was followed by another wash prior to mounting in 50% glycerol. Images were acquired using a Carl Zeiss AxioImager Z1 microscope and Apotome 2 optical sectioning or a Zeiss LSM 900 confocal microscope with Airyscan 2. Both systems run Zen acquisition software (Carl Zeiss Microscopy, Thornwood, NY, USA). Post acquisition, images were analyzed or further processed using FIJI (see below).

The p-Myosin/p-MRLC staining protocol was based on previously established protocols (Aranjuez et al., 2016; Lamb et al., 2021; Majumder et al., 2012). Briefly, ovarioles were fixed in 8% paraformaldehyde in 1× PBS and 0.5% Triton X-100 for 25 min at RT. Following fixation, samples were blocked in Triton antibody wash buffer (1× PBS, 0.5% Triton X-100 and 5% BSA) for 1–3 h. Ovarioles were incubated with primary antibodies for a minimum of 48 h at 4°C. Rabbit anti-phospho-myosin light chain 2 (Ser 19) antibody (3671T, Cell Signaling Technology, Danvers, MA, USA) was diluted 1:100 in Triton antibody wash buffer along with other antibodies and/or phalloidin as noted. This was followed by two to three 10-min washes in Triton antibody wash buffer and secondary antibody incubation overnight at 4°C (diluted 1:400 in Triton antibody wash buffer with or without phalloidin). Samples were washed once with Triton antibody wash buffer and incubated with DAPI as indicated (1:1000 diluted in 1× PBS), followed by mounting in 50% glycerol. Images were acquired using the Zeiss LSM 900 confocal microscope with Airyscan 2.

Live-imaging experiments were conducted similar to established protocols (Prasad et al., 2007) using genotypes as indicated in the figure legends. Egg chambers were dissected in dissection medium supplemented with 200 µg/ml insulin (Cell Applications, 128-100). Post dissection, egg chambers were transferred to fresh dissection medium, with or without 5 µg/ml FM4-64 (Thermo Fisher Scientific, T13320), a lipophilic dye to stain cell membranes. For analysis of border cell migration speed, egg chambers were imaged using the Carl Zeiss AxioImager Z1 microscope with a 20× objective every 3 min. For protrusion analysis, egg chambers were imaged using the Zeiss LSM 900 confocal microscope using a Plan-Apochromat 40×/1.20 N/A objective. Five to six *z*-planes spanning the border cell cluster were captured every 3 min using laser percentages <1.5% to reduce phototoxicity.

Quantification of migration defects at stage 9 and stage 10 of egg chamber development

Migration defects at stage 9 were scored by comparing the position of the border cell cluster with that of follicle cells that surrounded the egg chamber. Clusters were considered delayed if they were more than one nurse cell nucleus length away from the anteroposterior position where nurse cell-associated outer stretch cells meet with the columnar follicle cell line (Fig. S1A).

Migration defects at stage 10 were scored by comparing the position of the cluster with the oocyte border. Any cluster that had not reached the oocyte border by stage 10 was considered delayed. The approximate position of delayed clusters was estimated along the total migratory path (Fig. 1J′). Egg chambers were staged based on the position of the centripetal cells – at stage 10, the centripetal cells migrate inward and are aligned with the oocyte. In some cases, expression of GFP by the Gal4 line *slbo*-Gal4, UAS-mCD8-GFP was used to identify stage 10 egg chambers.

Quantification of border cell migration speeds

Migration speeds were quantified from timelapse videos of live-imaged egg chambers. A line was drawn from the anterior tip of the egg chamber to the middle of the cluster at the first and last frames of the videos. The difference in line lengths between the first and last frames was considered equal to the distance migrated. This was divided by the duration of the video in minutes to calculate speed of migration. For genotypes with detachment defects, undetached clusters were not included; only detached clusters were used for migration speed calculations.

Protrusion analysis

Protrusions were identified manually using PLCδ-PH–EGFP expression in sum-intensity z-projections of timelapse videos of live-imaged egg chambers. This construct fuses just the pleckstrin-homology (PH) domain

Journal of Cell Science (2024) 137, jcs261164. doi:10.1242/jcs.261164

of PLCδ to enhanced GFP, which recruits GFP to membranes by binding to phosphoinositides (Verstreken et al., 2009); thus, it has been used previously for protrusion analysis (Sawant et al., 2018). Both control and EcR-DN-expressing clusters were analyzed in the same way. Lengths of protrusions were measured using the Measure feature in FIJI. The length of a protrusion was calculated using a line drawn from the tip of the protrusion to the closest point along the periphery of the compact border cell cluster. Lifetime was defined as the duration between the first and the last time frame in which the protrusion was visible. If a protrusion was visible for a single frame only, the time interval of imaging was used as its lifetime. The direction of protrusion extension was identified by diving the cluster into four quadrants – forward, lateral top and bottom, and rear, as schematized in Fig. 2J. We did not track the dorsal or ventral orientations of the egg chambers, so 'top' and 'bottom' refer simply to the orientation in the images that we acquired.

Aspect ratio and perimeter analyses

For both aspect ratio and perimeter analyses, *slbo*-Gal4, UAS-mCD8-GFP flies were crossed to either w^{1118} (used as controls) or EcR-DN flies. Aspect ratio analysis was performed in FIJI. Sum-intensity z-projections of border cell clusters were duplicated and thresholded by adjusting the slider in default mode. Next, the thresholded image was converted to a binary image, followed by a single round of close operation and open operation (in the Process→Binary menu). These operations smoothen objects, fill in small holes and remove isolated pixels. The resulting image was converted to a mask, selected using the wand tool and added to the region-of-interest (ROI) manager. The ROI was measured with the following options selected in Analyze→Set Measurements: Area, Perimeter and Shape Descriptors. Use of sum-intensity z-projections ensured that protrusions extended by the cluster did not interfere with aspect ratio measurements.

Perimeter analysis was performed in a similar manner except that maximum-intensity projections were used. The perimeter of each cluster was normalized to its area for comparison across genotypes and stages of development. Use of maximum-intensity projections ensured that any protrusions that extended were taken into account.

Fluorescence signal distribution and intensity analysis

For E-cad distribution of antibody-stained egg chambers (Fig. 3A–D‴), the mean nurse cell cytoplasmic background was calculated in FIJI by drawing an ROI in the nurse cell cytoplasm and using Analyze→Histogram. Mean+(3×standard deviation) was subtracted from the image using Process→Math→Subtract. Following this, the '16 colors' lookup table (LUT) was applied to the background-subtracted image to generate a heatmap of distribution. The samples used were all stained under the same conditions and images were acquired under the same settings.

For aPKC and Dlg1 distributions of antibody-stained egg chambers, we conducted comparisons and acquired measurements for some genotypes. As a positive control and comparison to EcR-DN-mutant clusters, we examined Dlg1 distribution upon its overexpression using two different lines: EY05003 and *dlg1*-S48S, which should express the full-length coding regions of the protein under Gal4 activation (see Fig. S4 and Table S1). For measuring intensity and distribution of aPKC and Dlg1 expression using antibody staining in control and EcR-DN-mutant clusters (Fig. 4B,D,F,H), we used a freehand selection ROI with a 5 pt width line to outline the cluster in a *z*-plane containing the polar cells in FIJI. The outline started and ended at the middle of the apical side of the cluster as this was clearly detectable from the polar cells. This outline was then applied to a maximum-intensity projection of the cluster to measure fluorescence intensity along the circumference of the cluster using the Multi Plot tool. The resulting intensity measurements were scaled using minimum–maximum normalization. The scaled values (0–1) were plotted on the *y*-axis against normalized distance around the circumference and on the *x*-axis as a 0–1 range, where 0 marks the start of the freehand selection and 1 marks the end, as shown in Fig. 4 and Fig. S4.

Fluorescence intensities were measured using two separate methods. Images used in quantitative comparisons were all stained and acquired under the same conditions and settings.

EcR, E-cad, Hts and phalloidin levels (Fig. S1B–D; Fig. 3F; Fig. S3E-I) were quantified by adapting the corrected total cell fluorescence (CTCF) protocol described by McCloy et al. (2014) and obtained from The Open Lab Book. Briefly, for EcR (Fig. S3E), a freehand selection ROI was drawn outlining nuclei based on DAPI signal in FIJI. For phalloidin and Hts (Fig. S3H,I, respectively), a freehand selection ROI was drawn outlining the cluster. These ROIs were used to calculate area, mean, integrated density and raw integrated density (Analyze→Set Measurements: Area, integrated density, mean gray value). Separately, a circle ROI was drawn in the nurse cell cytoplasmic area to calculate background intensity. CTCF was calculated as the integrated density of freehand/line ROI–(area of freehand/line ROI×mean gray value of background ROI). The resulting CTCF values were normalized to DAPI or GFP CTCF values at the same locations for each nucleus or cluster, respectively, before plotting. For phalloidin and Hts, the normalized mean intensity of the control genotype was set to 1 to plot the data in GraphPad Prism.

E-cad antibody staining intensities (Fig. 3F; Fig. S3B–D) were calculated for each face of the cluster. A 5 pt width line ROI was drawn at the face being measured. Separately, a line ROI of the same length was drawn in the nurse cell cytoplasmic area to measure background intensity. Average intensities were calculated by subtracting average background intensities from average intensities at each face. For clusters where the background intensities were higher than the signal intensities (such as for clusters expressing E-cad RNAi), the average intensity after background subtraction was transformed by the lowest value+1 to make all values positive. This was repeated for the GFP expression. Finally, normalized mean intensity of the control genotype was set to 1 to plot the data.

Myosin, pMRLC foci counts and average foci area quantification

To examine myosin protein distribution, we used a *sqh*-GFP insertion line that expresses the *sqh* coding region with a GFP tag using the endogenous *sqh* promoter (Royou et al., 2004). For pMRLC foci analysis, maximum-intensity *z*-projections were analyzed in FIJI. A rectangular ROI was drawn in nurse cell cytoplasmic area and used to calculate background intensity using the Analyze→Histogram function. After background subtraction, the difference of Gaussian method was employed to create a mask of the image. Briefly, two duplicate images were created with a Gaussian blur filter of 1.00 sigma (radius) and 2.00 sigma (radius), respectively. The image with 2.00 sigma (radius) was subtracted from 1.00 sigma (radius) using the Image Calculator function. The resulting image with more discrete foci was thresholded using the default mode (the slider was adjusted where necessary by manual comparison with the original image). The thresholded image was converted to a mask. A bounding rectangle ROI was drawn around the cluster. The following options were selected in Analyze→Set Measurements: limit to threshold, bounding rectangle, area, area fraction. Finally, the Analyze particles function was used with a size range of 0.1 μm^2–∞ with the Show outlines option selected. The resulting outlines of foci were manually classified into quadrants – forward, lateral top and bottom, and rear. Quadrants were drawn on the cluster using the 'drawCirclesAndQuadrants.ijm' macro by Olivier Burri (https://gist.github.com/lacan/8acb3bfe51eb1b1ba6c60fba75e085a8).

Quantitative real-time PCR analysis

GR1-Gal4 virgin female flies were crossed with mCherry RNAi or w^{1118} (controls) or *usp* RNAi lines at 25°C. F1 progeny were fattened at 29°C overnight and ovaries were pooled from approximately five female flies. RNA was extracted using the RNeasy mini kit (Qiagen, 74104) with DNase I digestion (Thermo Fisher Scientific, EN0521). Following RNA extraction, cDNA was synthesized using 1 µg of RNA (Bio-Rad iScript cDNA synthesis kit, 1708841). Quantitative real-time PCR reactions were performed in triplicate with iTaq Universal SYBR Green Supermix (Bio-Rad, 1725122) and primers targeting *usp* and *RpL32* (also known as *rp49*); the latter was used as the reference gene. *usp* primers were designed according to the fly primer bank (Hu et al., 2013). The primer sequences were: *usp* forward 1, 5′-CAGCATCGTTTCGCTGGATG-3′; *usp* reverse 1, 5′-TGCGATGGTACGAGAAGCTC-3′; *usp* forward 2, 5′-CAGCAGCTT-TTCGCCCAAG-3′; *usp* reverse 2, 5′-CGATCCCCGCAAATAGAGCA-3′, *RpL32* forward, 5′-TATTCCGACCACGTTACAAG-3′; and *RpL32*

reverse, 5′-AGCATACAGGCCCAAGATC-3′. A Bio-Rad CFX96 qPCR instrument was used to detect differences in RNA levels. Three biological replicates were performed.

Software

Zen acquisition software (v3.6, Carl Zeiss Microscopy) was used to view and acquire images. FIJI (v1.54b and v1.54f) was used for image analysis, post image processing and movie generation. GraphPad Prism (v9.5.1 and v10.1.0 for Windows, GraphPad Software, San Diego, CA, USA) was used for statistical analysis and graph production. Statistical tests used are indicated in figure legends.

Acknowledgements

We are grateful to Dr Jocelyn McDonald and the Bloomington *Drosophila* Stock Center (National Institutes of Health, P40OD018537) for fly stocks, Dr Pernille Rorth and the Developmental Studies Hybridoma Bank at the University of Iowa for antibodies as listed, and FlyBase for providing genetic and stock information, and for database management and maintenance (Gramates et al., 2022). Furthermore, we would like to thank Dr Tagide DeCarvalho and the Keith Porter Imaging Facility for microscopy training and assistance with image export and analysis. We also thank Alexander George and Sabeen Ikram for critically reading the manuscript and helpful discussion.

Competing interests

The authors declare no competing or financial interests.

Author contributions

Conceptualization: M.B., M.S.-G.; Methodology: M.B.; Software: M.B.; Validation: M.B.; Formal analysis: M.B., M.S.-G.; Investigation: M.B., M.S.-G.; Resources: M.S.-G.; Data curation: M.B.; Writing - original draft: M.B.; Writing - review & editing: M.B., M.S.-G.; Visualization: M.B.; Supervision: M.S.-G.; Project administration: M.S.-G.; Funding acquisition: M.S.-G..

Funding

This work was supported in part by the National Science Foundation (NSF) grants IOS-656550 to M.S.-G. and NIGMS-NSF-DMS-1953423 to M.S.-G. and Dr Bradford Peercy (University of Maryland Baltimore County).

Data availability

All relevant data can be found within the article and its supplementary information.

Peer review history

The peer review history is available online at https://journals.biologists.com/jcs/lookup/doi/10.1242/jcs.261164.reviewer-comments.pdf

References

Alhadyian, H., Shoaib, D. and Ward, R. E. (2021). Septate junction proteins are required for egg elongation and border cell migration during oogenesis in Drosophila. *G3* **11**, jkab127. doi:10.1093/g3journal/jkab127

Aman, A. and Piotrowski, T. (2010). Cell migration during morphogenesis. *Dev. Biol.* **341**, 20-33. doi:10.1016/j.ydbio.2009.11.014

Anllo, L. and Schüpbach, T. (2016). Signaling through the G-protein-coupled receptor Rickets is important for polarity, detachment, and migration of the border cells in Drosophila. *Dev. Biol.* **414**, 193-206. doi:10.1016/j.ydbio.2016.04.017

Ann Mack, N. and Georgiou, M. (2014). The interdependence of the Rho GTPases and apicobasal cell polarity. *Small GTPases* **5**, 10. doi:10.4161/21541248.2014.973768

Aranjuez, G., Burtscher, A., Sawant, K., Majumder, P. and McDonald, J. A. (2016). Dynamic myosin activation promotes collective morphology and migration by locally balancing oppositional forces from surrounding tissue. *Mol. Biol. Cell* **27**, 1898-1910. doi:10.1091/mbc.e15-10-0744

Bai, J., Uehara, Y. and Montell, D. J. (2000). Regulation of invasive cell behavior by taiman, a Drosophila protein related to AIB1, a steroid receptor coactivator amplified in breast cancer. *Cell* **103**, 1047-1058. doi:10.1016/S0092-8674(00)00208-7

Bastock, R. and Strutt, D. (2007). The planar polarity pathway promotes coordinated cell migration during Drosophila oogenesis. *Development* **134**, 3055-3064. doi:10.1242/dev.010447

Bazellières, E., Aksenova, V., Barthélémy-Requin, M., Massey-Harroche, D. and Le Bivic, A. (2018). Role of the Crumbs proteins in ciliogenesis, cell migration and actin organization. *Semin. Cell Dev. Biol.* **81**, 13-20. doi:10.1016/j.semcdb.2017.10.018

Bianco, A., Poukkula, M., Cliffe, A., Mathieu, J., Luque, C. M., Fulga, T. A. and Rørth, P. (2007). Two distinct modes of guidance signalling during collective migration of border cells. *Nature* **448**, 362-365. doi:10.1038/nature05965

Bilder, D., Schober, M. and Perrimon, N. (2002). Integrated activity of PDZ protein complexes regulates epithelial polarity. *Nat. Cell Biol.* **5**, 53-58. doi:10.1038/ncb897

Blackley, D. G., Cooper, J. H., Pokorska, P. and Ratheesh, A. (2021). Mechanics of developmental migration. *Semin. Cell Dev. Biol.* **120**, 66-74. doi:10.1016/j.semcdb.2021.07.002

Buckley, C. E. and St Johnston, D. (2022). Apical–basal polarity and the control of epithelial form and function. *Nat. Rev. Mol. Cell Biol.* **23**, 559-577. doi:10.1038/s41580-022-00465-y

Buszczak, M., Freeman, M. R., Carlson, J. R., Bender, M., Cooley, L. and Segraves, W. A. (1999). Ecdysone response genes govern egg chamber development during mid-oogenesis in Drosophila. *Development* **126**, 4581-4589. doi:10.1242/dev.126.20.4581

Cai, D., Chen, S.-C., Prasad, M., He, L., Wang, X., Choesmel-Cadamuro, V., Sawyer, J. K., Danuser, G. and Montell, D. J. (2014). Mechanical feedback through E-cadherin promotes direction sensing during collective cell migration. *Cell* **157**, 1146-1159. doi:10.1016/j.cell.2014.03.045

Campanale, J. P., Mondo, J. A. and Montell, D. J. (2022). A Scribble/Cdep/Rac pathway controls follower-cell crawling and cluster cohesion during collective border-cell migration. *Dev. Cell* **57**, 2483-2496.e4. doi:10.1016/j.devcel.2022.10.004

Cavey, M., Rauzi, M., Lenne, P.-F. and Lecuit, T. (2008). A two-tiered mechanism for stabilization and immobilization of E-cadherin. *Nature* **453**, 751-756. doi:10.1038/nature06953

Chen, Y., Kotian, N., Aranjuez, G., Chen, L., Messer, C. L., Burtscher, A., Sawant, K., Ramel, D., Wang, X. and McDonald, J. A. (2020). Protein phosphatase 1 activity controls a balance between collective and single cell modes of migration. *eLife* **9**, e52979. doi:10.7554/eLife.52979

Chen, Y., Brasch, J., Harrison, O. J. and Bidone, T. C. (2021). Computational model of E-cadherin clustering under force. *Biophys. J.* **120**, 4944-4954. doi:10.1016/j.bpj.2021.10.018

Cherbas, L., Hu, X., Zhimulev, I., Belyaeva, E. and Cherbas, P. (2003). EcR isoforms in Drosophila: testing tissue-specific requirements by targeted blockade and rescue. *Development* **130**, 271-284. doi:10.1242/dev.00205

DaCrema, D., Bhandari, R., Karanja, F., Yano, R. and Halme, A. (2021). Ecdysone regulates the Drosophila imaginal disc epithelial barrier, determining the length of regeneration checkpoint delay. *Development* **148**, dev195057. doi:10.1242/dev.195057

Dai, W., Guo, X., Cao, Y., Mondo, J. A., Campanale, J. P., Montell, B. J., Burrous, H., Streichan, S., Gov, N., Rappel, W.-J. et al. (2020). Tissue topography steers migrating Drosophila border cells. *Science* **370**, 987-990. doi:10.1126/science.aaz4741

Dawson, M. I. and Xia, Z. (2012). The retinoid X receptors and their ligands. *Biochim. Biophys. Acta* **1821**, 21-56. doi:10.1016/j.bbalip.2011.09.014

Domanitskaya, E., Anllo, L. and Schüpbach, T. (2014). Phantom, a cytochrome P450 enzyme essential for ecdysone biosynthesis, plays a critical role in the control of border cell migration in Drosophila. *Dev. Biol.* **386**, 408-418. doi:10.1016/j.ydbio.2013.12.013

Edwards, K. A. and Kiehart, D. P. (1996). Drosophila nonmuscle myosin II has multiple essential roles in imaginal disc and egg chamber morphogenesis. *Development* **122**, 1499-1511. doi:10.1242/dev.122.5.1499

Etienne-Manneville, S. (2012). Adherens junctions during cell migration. In *Adherens Junctions: From Molecular Mechanisms to Tissue Development and Disease. Sub-Cellular Biochemistry* (ed. T. Harris), pp. 225-249. Dordrecht: Springer. doi:10.1007/978-94-007-4186-7_10

Felix, M., Chayengia, M., Ghosh, R., Sharma, A. and Prasad, M. (2015). Pak3 regulates apical-basal polarity in migrating border cells during Drosophila oogenesis. *Dev.* **142**, 3692-3703. doi:10.1242/dev.125682

Förster, C., Mäkela, S., Wärri, A., Kietz, S., Becker, D., Hultenby, K., Warner, M. and Gustafsson, J.-Å. (2002). Involvement of estrogen receptor β in terminal differentiation of mammary gland epithelium. *Proc. Natl. Acad. Sci. USA* **99**, 15578-15583. doi:10.1073/pnas.192561299

Friedl, P. and Mayor, R. (2017). Tuning collective cell migration by cell–cell junction regulation. *Cold Spring Harb. Perspect. Biol.* **9**, a029199. doi:10.1101/cshperspect.a029199

Fulga, T. A. and Rørth, P. (2002). Invasive cell migration is initiated by guided growth of long cellular extensions. *Nat. Cell Biol.* **4**, 715-719. doi:10.1038/ncb848

Gandalovičová, A., Vomastek, T., Rosel, D., Brábek, J., Gandalovičová, A., Vomastek, T., Rosel, D. and Brábek, J. (2016). Cell polarity signaling in the plasticity of cancer cell invasiveness. *Oncotarget* **7**, 25022-25049. doi:10.18632/oncotarget.7214

Gates, J., Nowotarski, S. H., Yin, H., Mahaffey, J. P., Bridges, T., Herrera, C., Homem, C. C. F., Janody, F., Montell, D. J. and Peifer, M. (2009). Enabled and Capping protein play important roles in shaping cell behavior during Drosophila oogenesis. *Dev. Biol.* **333**, 90-107. doi:10.1016/j.ydbio.2009.06.030

Giedt, M. S. and Tootle, T. L. (2023). The vast utility of Drosophila oogenesis. *Methods Mol. Biol.* **2626**, 1-36. doi:10.1007/978-1-0716-2970-3_1

Goode, S. and Perrimon, N. (1997). Inhibition of patterned cell shape change and cell invasion by Discs large during Drosophila oogenesis. *Genes Dev.* **11**, 2532-2544. doi:10.1101/gad.11.19.2532
Gramates, L. S., Agapite, J., Attrill, H., Calvi, B. R., Crosby, M. A., dos Santos, G., Goodman, J. L., Goutte-Gattat, D., Jenkins, V. K., Kaufman, T. et al. (2022). FlyBase: a guided tour of highlighted features. *Genetics* **220**, iyac035. doi:10.1093/genetics/iyac035
Grammont, M. (2007). Adherens junction remodeling by the Notch pathway in Drosophila melanogaster oogenesis. *J. Cell Biol.* **177**, 139-150. doi:10.1083/jcb.200609079
Gupta, T. and Schüpbach, T. (2003). Cct1, a phosphatidylcholine biosynthesis enzyme, is required for Drosophila oogenesis and ovarian morphogenesis. *Development* **130**, 6075-6087. doi:10.1242/dev.00817
Hackney, J. F., Pucci, C., Naes, E. and Dobens, L. (2007). Ras signaling modulates activity of the ecdysone receptor EcR during cell migration in the drosophila ovary. *Dev. Dyn.* **236**, 1213-1226. doi:10.1002/dvdy.21140
Helguero, L. A., Lindberg, K., Gardmo, C., Schwend, T., Gustafsson, J.-Å. and Haldosén, L.-A. (2008). Different roles of estrogen receptors α and β in the regulation of e-cadherin protein levels in a mouse mammary epithelial cell line. *Cancer Res.* **68**, 8695-8704. doi:10.1158/0008-5472.CAN-08-0788
Hong, S., Troyanovsky, R. B. and Troyanovsky, S. M. (2013). Binding to F-actin guides cadherin cluster assembly, stability, and movement. *J. Cell Biol.* **201**, 131-143. doi:10.1083/jcb.201211054
Hu, X., Cherbas, L. and Cherbas, P. (2003). Transcription Activation by the Ecdysone Receptor (EcR/USP): identification of activation functions. *Mol. Endocrinol.* **17**, 716-731. doi:10.1210/me.2002-0287
Hu, Y., Sopko, R., Foos, M., Kelley, C., Flockhart, I., Ammeux, N., Wang, X., Perkins, L., Perrimon, N. and Mohr, S. E. (2013). FlyPrimerBank: an online database for Drosophila melanogaster gene expression analysis and knockdown evaluation of RNAi reagents. *G3 (Bethesda)* **3**, 1607-1616. doi:10.1534/g3.113.007021
Huang, J., Zhou, W., Dong, W., Watson, A. M. and Hong, Y. (2009). Directed, efficient, and versatile modifications of the Drosophila genome by genomic engineering. *Proc. Natl. Acad. Sci. USA* **106**, 8284-8289. doi:10.1073/pnas.0900641106
Hudson, A. M. and Cooley, L. (2014). Methods for studying oogenesis. *Methods* **68**, 207-217. doi:10.1016/j.ymeth.2014.01.005
Jang, A. C.-C., Chang, Y.-C., Bai, J. and Montell, D. (2009). Border-cell migration requires integration of spatial and temporal signals by the BTB protein Abrupt. *Nat. Cell Biol.* **11**, 569-579. doi:10.1038/ncb1863
Karess, R. E., Chang, X.-J., Edwards, K. A., Kulkarni, S., Aguilera, I. and Kiehart, D. P. (1991). The regulatory light chain of nonmuscle myosin is encoded by spaghetti-squash, a gene required for cytokinesis in Drosophila. *Cell* **65**, 1177-1189. doi:10.1016/0092-8674(91)90013-O
Kawata, M., Kondo, J., Onuma, K., Ito, Y., Yokoi, T., Hamanishi, J., Mandai, M., Kimura, T. and Inoue, M. (2022). Polarity switching of ovarian cancer cell clusters via SRC family kinase is involved in the peritoneal dissemination. *Cancer Sci.* **113**, 3437-3448. doi:10.1111/cas.15493
Khadilkar, R. J. and Tanentzapf, G. (2019). Septate junction components control drosophila hematopoiesis through the hippo pathway. *Development* **146**, dev166819. doi:10.1242/dev.166819
Kim, J. H., Cho, A., Yin, H., Schafer, D. A., Mouneimne, G., Simpson, K. J., Nguyen, K.-V., Brugge, J. S. and Montell, D. J. (2011). Psidin, a conserved protein that regulates protrusion dynamics and cell migration. *Genes Dev.* **25**, 730-741. doi:10.1101/gad.2028611
King, R. C. (1970). Ovarian Development in *Drosophila melanogaster*. Academic Press, New York.
Kittler, R., Zhou, J., Hua, S., Ma, L., Liu, Y., Pendleton, E., Cheng, C., Gerstein, M. and White, K. (2013). A comprehensive nuclear receptor network for breast cancer cells. *Cell Rep.* **3**, 538-551. doi:10.1016/j.celrep.2013.01.004
Lamb, M. C., Anliker, K. K. and Tootle, T. L. (2020). Fascin regulates protrusions and delamination to mediate invasive, collective cell migration *in vivo*. *Dev. Dyn.* **249**, 961-982. doi:10.1002/dvdy.186
Lamb, M. C., Kaluarachchi, C. P., Lansakara, T. I., Mellentine, S. Q., Lan, Y., Tivanski, A. V. and Tootle, T. L. (2021). Fascin limits Myosin activity within Drosophila border cells to control substrate stiffness and promote migration. *eLife* **10**, e69836. doi:10.7554/eLife.69836
Lee, A. and Treisman, J. E. (2004). Excessive myosin activity in Mbs mutants causes photoreceptor movement out of the Drosophila eye disc epithelium. *Mol. Biol. Cell* **15**, 3285-3295. doi:10.1091/mbc.e04-01-0057
Li, Y., Haynes, P., Zhang, S. L., Yue, Z. and Sehgal, A. (2023). Ecdysone acts through cortex glia to regulate sleep in Drosophila. *eLife* **12**, e81723. doi:10.7554/eLife.81723
Majumder, P., Aranjuez, G., Amick, J. and McDonald, J. A. (2012). Par-1 controls myosin-II activity through myosin phosphatase to regulate border cell migration. *Curr. Biol.* **22**, 363-372. doi:10.1016/j.cub.2012.01.037
Manning, L., Sheth, J., Bridges, S., Saadin, A., Odinammadu, K., Andrew, D., Spencer, S., Montell, D. and Starz-Gaiano, M. (2017). A hormonal cue promotes timely follicle cell migration by modulating transcription profiles. *Mech. Dev.* **148**, 56-68. doi:10.1016/j.mod.2017.06.003
McCloy, R. A., Rogers, S., Caldon, C. E., Lorca, T., Castro, A. and Burgess, A. (2014). Partial inhibition of Cdk1 in G2 phase overrides the SAC and decouples mitotic events. *Cell Cycle* **13**, 1400-1412. doi:10.4161/cc.28401
McDonald, J. A., Khodyakova, A., Aranjuez, G., Dudley, C. and Montell, D. J. (2008). PAR-1 kinase regulates epithelial detachment and directional protrusion of migrating border cells. *Curr. Biol.* **18**, 1659-1667. doi:10.1016/j.cub.2008.09.041
Mège, R. M. and Ishiyama, N. (2017). Integration of cadherin adhesion and cytoskeleton at adherens junctions. *Cold Spring Harb. Perspect. Biol.* **9**, a028738. doi:10.1101/cshperspect.a028738
Mishra, A. K., Mondo, J. A., Campanale, J. P. and Montell, D. J. (2019). Coordination of protrusion dynamics within and between collectively migrating border cells by myosin II. *Mol. Biol. Cell* **30**, 2490-2502. doi:10.1091/mbc.E19-02-0124
Montell, D. J., Rorth, P. and Spradling, A. C. (1992). slow border cells, a locus required for a developmentally regulated cell migration during oogenesis, encodes Drosophila C/EBP. *Cell* **71**, 51-62. doi:10.1016/0092-8674(92)90265-E
Montell, D. J., Yoon, W. H. and Starz-Gaiano, M. (2012). Group choreography: mechanisms orchestrating the collective movement of border cells. *Nat. Rev. Mol. Cell Biol.* **13**, 631-645. doi:10.1038/nrm3433
Murphy, A. M. and Montell, D. J. (1996). Cell type-specific roles for Cdc42, Rac, and Rhol in Drosophila oogenesis. *J. Cell Biol.* **133**, 617-630. doi:10.1083/jcb.133.3.617
Ni, J.-Q., Zhou, R., Czech, B., Liu, L.-P., Holderbaum, L., Yang-Zhou, D., Shim, H.-S., Tao, R., Handler, D., Karpowicz, P. et al. (2011). A genome-scale shRNA resource for transgenic RNAi in Drosophila. *Nat. Methods* **8**, 405-407. doi:10.1038/nmeth.1592
Niewiadomska, P., Godt, D. and Tepass, U. (1999). DE-Cadherin is required for intercellular motility during Drosophila oogenesis. *J. Cell Biol.* **144**, 533-547. doi:10.1083/jcb.144.3.533
Oda, H., Uemura, T., Harada, Y., Iwai, Y. and Takeichi, M. (1994). A Drosophila homolog of cadherin associated with armadillo and essential for embryonic cell-cell adhesion. *Dev. Biol.* **165**, 716-726. doi:10.1006/dbio.1994.1287
Oda, H., Tsukita, S. and Takeichi, M. (1998). Dynamic behavior of the cadherin-based cell–cell adhesion system during Drosophila gastrulation. *Dev. Biol.* **203**, 435-450. doi:10.1006/dbio.1998.9047
Okuyama, H., Kondo, J., Sato, Y., Endo, H., Nakajima, A., Piulats, J. M., Tomita, Y., Fujiwara, T., Itoh, Y., Mizoguchi, A. et al. (2016). Dynamic change of polarity in primary cultured spheroids of human colorectal adenocarcinoma and its role in metastasis. *Am. J. Pathol.* **186**, 899-911. doi:10.1016/j.ajpath.2015.12.011
Oshima, K. and Fehon, R. G. (2011). Analysis of protein dynamics within the septate junction reveals a highly stable core protein complex that does not include the basolateral polarity protein Discs large. *J. Cell Sci.* **124**, 2861-2871. doi:10.1242/jcs.087700
Peercy, B. E. and Starz-Gaiano, M. (2020). Clustered cell migration: modeling the model system of Drosophila border cells. *Semin. Cell Dev. Biol.* **100**, 167-176. doi:10.1016/j.semcdb.2019.11.010
Peifer, M. and Wleschaus, E. (1990). The segment polarity gene armadillo encodes a functionally modular protein that is the Drosophila homolog of human plakoglobin. *Cell* **63**, 1167-1178. doi:10.1016/0092-8674(90)90413-9
Pinheiro, E. M. and Montell, D. J. (2004). Requirement for Par-6 and Bazooka in Drosophila border cell migration. *Development* **131**, 5243-5251. doi:10.1242/dev.01412
Plutoni, C., Keil, S., Zeledon, C., Delsin, L. E. A., Decelle, B., Roux, P. P., Carréno, S. and Emery, G. (2019). Misshapen coordinates protrusion restriction and actomyosin contractility during collective cell migration. *Nat. Commun.* **10**, 3940. doi:10.1038/s41467-019-11963-7
Polvani, S., Tarocchi, M., Tempesti, S. and Galli, A. (2014). Nuclear receptors and pathogenesis of pancreatic cancer. *World J. Gastroenterol.* **20**, 12062-12081. doi:10.3748/wjg.v20.i34.12062
Poukkula, M., Cliffe, A., Changede, R. and Rørth, P. (2011). Cell behaviors regulated by guidance cues in collective migration of border cells. *J. Cell Biol.* **192**, 513-524. doi:10.1083/jcb.201010003
Prasad, M. and Montell, D. J. (2007). Cellular and molecular mechanisms of border cell migration analyzed using time-lapse live-cell imaging. *Dev. Cell* **12**, 997-1005. doi:10.1016/j.devcel.2007.03.021
Prasad, M., Jang, A. C.-C., Starz-Gaiano, M., Melani, M. and Montell, D. J. (2007). A protocol for culturing Drosophila melanogaster stage 9 egg chambers for live imaging. *Nat. Protoc.* **2**, 2467-2473. doi:10.1038/nprot.2007.363
Rice, C., De, O., Alhadyian, H., Hall, S. and Ward, R. E. (2021). Expanding the Junction: New Insights into Non-Occluding Roles for Septate Junction Proteins during Development. *J. Dev. Biol.* **9**, 11. doi:10.3390/jdb9010011
Riddiford, L. M. (1993). Hormones and Drosophila development. In *The Development of Drosophila Melanogaster* (ed. M. Bate and A. M. Arias). pp. 899-939. Cold Spring Harbor Laboratory Press.
Roberto, G. M. and Emery, G. (2022). Directing with restraint: mechanisms of protrusion restriction in collective cell migrations. *Semin. Cell Dev. Biol.* **129**, 75-81. doi:10.1016/j.semcdb.2022.03.037
Romani, P., Bernardi, F., Hackney, J., Dobens, L., Gargiulo, G. and Cavaliere, V. (2009). Cell survival and polarity of Drosophila follicle cells require the activity of

ecdysone receptor B1 isoform. *Genetics* **181**, 165-175. doi:10.1534/genetics.108.096008

Royou, A., Field, C., Sisson, J. C., Sullivan, W. and Karess, R. (2004). Reassessing the role and dynamics of nonmuscle myosin II during furrow formation in early Drosophila embryos. *Mol. Biol. Cell* **15**, 838-850. doi:10.1091/mbc.e03-06-0440

Saadin, A. and Starz-Gaiano, M. (2016). Circuitous genetic regulation governs a straightforward cell migration. *Trends Genet.* **32**, 660-673. doi:10.1016/j.tig.2016.08.001

Sawant, K., Chen, Y., Kotian, N., Preuss, K. M. and McDonald, J. A. (2018). Rap1 GTPase promotes coordinated collective cell migration in vivo. *Mol. Biol. Cell* **29**, 2656-2673. doi:10.1091/mbc.E17-12-0752

Schäfer, G., Narasimha, M., Vogelsang, E. and Leptin, M. (2014). Cadherin switching during the formation and differentiation of the Drosophila mesoderm - implications for epithelial-to-mesenchymal transitions. *J. Cell Sci.* **141**, e0907. doi:10.1242/dev.110882

Schober, M., Rebay, I. and Perrimon, N. (2005). Function of the ETS transcription factor Yan in border cell migration. *Development* **132**, 3493-3504. doi:10.1242/dev.01911

Shellard, A. and Mayor, R. (2019). Supracellular migration - beyond collective cell migration. *J. Cell Sci.* **132**, jcs226142. doi:10.1242/jcs.226142

Stephens, R., Lim, K., Portela, M., Kvansakul, M., Humbert, P. O. and Richardson, H. E. (2018). The scribble cell polarity module in the regulation of cell signaling in tissue development and tumorigenesis. *J. Mol. Biol.* **430**, 3585-3612. doi:10.1016/j.jmb.2018.01.011

Stonko, D. P., Manning, L., Starz-Gaiano, M. and Peercy, B. E. (2015). A mathematical model of collective cell migration in a three-dimensional, heterogeneous environment. *PLoS ONE* **10**, e0122799. doi:10.1371/journal.pone.0122799

Tanentzapf, G. and Tepass, U. (2002). Interactions between the crumbs, lethal giant larvae and bazooka pathways in epithelial polarization. *Nat. Cell Biol.* **5**, 46-52. doi:10.1038/ncb896

Tekotte, H., Tollervey, D. and Davis, I. (2007). Imaging the migrating border cell cluster in living Drosophila egg chambers. *Dev. Dyn.* **236**, 2818-2824. doi:10.1002/dvdy.21305

Theveneau, E. and Mayor, R. (2013). Collective cell migration of epithelial and mesenchymal cells. *Cell. Mol. Life Sci.* **70**, 3481-3492. doi:10.1007/s00018-012-1251-7

Theveneau, E., Marchant, L., Kuriyama, S., Gull, M., Moepps, B., Parsons, M. and Mayor, R. (2010). Collective chemotaxis requires contact-dependent cell polarity. *Dev. Cell* **19**, 39-53. doi:10.1016/j.devcel.2010.06.012

Theveneau, E., Steventon, B., Scarpa, E., Garcia, S., Trepat, X., Streit, A. and Mayor, R. (2013). Chase-and-run between adjacent cell populations promotes directional collective migration. *Nat. Cell Biol.* **15**, 763-772. doi:10.1038/ncb2772

Thomas, H. E., Stunnenberg, H. G. and Stewart, A. F. (1993). Heterodimerization of the Drosophila ecdysone receptor with retinoid X receptor and ultraspiracle. *Nature* **362**, 471-475. doi:10.1038/362471a0

Tran, D. H. and Berg, C. A. (2003). bullwinkle and shark regulate dorsal-appendage morphogenesis in Drosophila oogenesis. *Development* **130**, 6273-6282. doi:10.1242/dev.00854

Truong Quang, B.-A., Mani, M., Markova, O., Lecuit, T. and Lenne, P.-F. (2013). Principles of E-cadherin supramolecular organization in vivo. *Curr. Biol.* **23**, 2197-2207. doi:10.1016/j.cub.2013.09.015

Veeman, M. T. and McDonald, J. A. (2016). Dynamics of cell polarity in tissue morphogenesis: a comparative view from *Drosophila* and *Ciona*. *F1000Research* **5**, 1084. doi:10.12688/f1000research.8011.1

Verstreken, P., Ohyama, T., Haueter, C., Habets, R. L. P., Lin, Y. Q., Swan, L. E., Ly, C. V., Venken, K. J. T., De Camilli, P. and Bellen, H. J. (2009). Tweek, an evolutionarily conserved protein, is required for synaptic vesicle recycling. *Neuron* **63**, 203-215. doi:10.1016/j.neuron.2009.06.017

Wada-Hiraike, O., Hiraike, H., Okinaga, H., Imamov, O., Barros, R. P. A., Morani, A., Omoto, Y., Warner, M. and Gustafsson, J.-Å. (2006). Role of estrogen receptor β in uterine stroma and epithelium: insights from estrogen receptor β–/– mice. *Proc. Natl. Acad. Sci. USA* **103**, 18350. doi:10.1073/pnas.0608861103

Wang, X., He, L., Wu, Y. I., Hahn, K. M. and Montell, D. J. (2010). Light-mediated activation reveals a key role for Rac in collective guidance of cell movement in vivo. *Nat. Cell Biol.* **12**, 591-597. doi:10.1038/ncb2061

Wang, H., Qiu, Z., Xu, Z., Chen, S. J., Luo, J., Wang, X. and Chen, J. (2018). aPKC is a key polarity determinant in coordinating the function of three distinct cell polarities during collective migration. *Development* **145**, dev158444. doi:10.1242/dev.158444

Wang, H., Guo, X., Wang, X., Wang, X. and Chen, J. (2020). Supracellular actomyosin mediates cell-cell communication and shapes collective migratory morphology. *IScience* **23**, 101204. doi:10.1016/j.isci.2020.101204

Woods, D. F. and Bryant, P. J. (1991). The discs-large tumor suppressor gene of Drosophila encodes a guanylate kinase homolog localized at septate junctions. *Cell* **66**, 451-464. doi:10.1016/0092-8674(81)90009-X

Woods, D. F., Hough, C., Peel, D., Callaini, G. and Bryant, P. J. (1996). Dlg protein is required for junction structure, cell polarity, and proliferation control in Drosophila epithelia. *J. Cell Biol.* **134**, 1469-1482. doi:10.1083/jcb.134.6.1469

Yamamoto, A., Doak, A. E. and Cheung, K. J. (2023). Orchestration of collective migration and metastasis by tumor cell clusters. **18**, 231-256. doi:10.1146/annurev-pathmechdis-031521-023557

Yao, T.-P., Forman, B. M., Jiang, Z., Cherbas, L., Chen, J.-D., McKeown, M., Cherbas, P. and Evans, R. M. (1993). Functional ecdysone receptor is the product of EcR and Ultraspiracle genes. *Nature* **366**, 476-479. doi:10.1038/366476a0

Zeledon, C., Sun, X., Plutoni, C. and Emery, G. (2019). The ArfGAP drongo promotes actomyosin contractility during collective cell migration by releasing myosin phosphatase from the trailing edge. *Cell Rep.* **28**, 3238-3248.e3. doi:10.1016/j.celrep.2019.08.044

Zhang, L., Luo, J., Wan, P., Wu, J., Laski, F. and Chen, J. (2011). Regulation of cofilin phosphorylation and asymmetry in collective cell migration during morphogenesis. *Development* **138**, 455-464. doi:10.1242/dev.046870

Zhao, X., Cho, H., Yu, R. T., Atkins, A. R., Downes, M. and Evans, R. M. (2014). Nuclear receptors rock around the clock. *EMBO Rep.* **15**, 518-528. doi:10.1002/embr.201338271